Rep. Prog. Phys. 60 (1997) 761–817. Printed in the UK PII: S0034-4885(97)34964-1

Trapped-ion and trapped-atom microwave frequency standards

Peter T H Fisk†

National Measurement Laboratory, CSIRO Division of Telecommunications and Industrial Physics, PO Box 218, Lindfield NSW 2070, Sydney, Australia

Received 23 January 1997

Abstract

The stability and accuracy of atomic microwave frequency standards (atomic clocks) have been improving at a rate exceeding one order of magnitude per decade for the past 30 years. This sustained improvement has been driven mainly by the many and diverse technological applications requiring highly stable and accurate time and frequency standards. There is no reason to suspect that this rate of progress is slowing.

Over the last decade, research and development in atomic frequency standards has tended increasingly towards the use of atom and ion trapping technologies to approach the supposedly ideal unperturbed atomic frequency reference consisting of a single atom or ion either motionless or in free-fall in a perfect, field-free vacuum. This work has been facilitated by the relatively recent development of techniques whereby laser light is used to cool, confine and manipulate atoms or ions.

This paper reviews the current status of atomic microwave frequency standards based on trapped atoms and trapped ions, and attempts to explain the motivation for their development and the principles of their operation, with particular emphasis on the physics of factors which limit their performance.

† E-mail address: Peter.Fisk@tip.csiro.au

0034-4885/97/080761+57$59.50

Contents

1. Introduction to atomic frequency standards

Atomic frequency standards, also known as atomic clocks, operate on the principle that atoms generally absorb or emit electromagnetic radiation at discrete frequencies, known as resonances or spectral lines. Some of these resonances are very spectrally narrow, their frequencies can be determined very precisely and are fundamentally reproducible. This reproducibility is in contrast to, for example, the case of a quartz oscillator or a pendulum, whose resonance frequencies depend, respectively, on the physical dimensions and properties of a quartz crystal or the length of a pendulum, both of which are man-made. An atomic frequency standard is a device whose output frequency is derived directly from the frequency of an atomic resonance, and ideally, the device is designed and constructed so as to minimize the influence of external environmental variations.

Although there are many species of atom which could, in principle, be used as a basis for an atomic frequency standard, commercially available standards currently use resonances in caesium (caesium beam standards), rubidium (rubidium standards) or hydrogen (hydrogen masers) to determine their output frequency. There are many technical reasons for the development of this situation, including the susceptibility of the resonant frequencies of the various atomic species to external perturbations, and the relative convenience with which the atoms can be prepared in a suitable form, for example, in an atomic beam (caesium standards) or a vapour (rubidium standards and hydrogen masers).

Despite the above considerations, the most important determining factor resulting in atomic frequency standards based on caesium, rubidium and hydrogen being developed into commercial devices is the fact that all three species have absorption resonances (table 1) suitable for standards purposes in the microwave region of the electromagnetic spectrum.

Although accurate measurement of frequency is important throughout the electromagnetic spectrum, the very different characteristics of propagation and interaction with matter of, for example, radiofrequency radiation (which can propagate in free space or along a cable) and gamma rays (to which many materials are transparent) has so far prevented the development of a system of frequency measurement and delivery which is homogeneous throughout the spectrum. Consequently, frequency standards in different regions of the electromagnetic spectrum have developed at vastly different rates, driven by technological requirements. For example, one of the most important applications for frequency standards is the measurement of time, with intervals of time being defined in terms of a number of cycles of electromagnetic radiation at a particular frequency. It is self evident that the higher

Table 1. Microwave absorption resonance frequencies of the three atomic species used in commercially available atomic microwave frequency standards. The frequency of the caesium standard is exact, because it has been chosen to define the Système Internationale (SI, or metric) second. From Vanier and Audion (1989, p 24).

Reference atom	Resonance frequency (Hz)
Caesium (^{133}Cs)	9192 631 770
Rubidium (^{87}Rb)	6834 682 612.8 ± 0.5
Hydrogen (^{1}H)	1420 405 751.770 ± 0.003

this frequency is, the more cycles are counted to define a particular time interval, and the more precisely this time interval will be determined. This consideration obviously favours the choice of an atomic transition in the optical frequency range or higher. However, the question arises as to how the cycles of the radiation are to be counted; a compact and reliable device for direct counting of cycles of optical radiation has not yet been developed. On the other hand, counting of cycles in the radiofrequency and microwave region is straightforward, and has led to the most commonly used and most highly developed frequency standards operating on atomic resonances in this region.

Another factor favouring the development of frequency standards in the microwave region is that applications requiring stable and reproducible frequencies usually also require a frequency that does not necessarily coincide with an atomic absorption resonance. For example, a television broadcasting station transmits on a frequency which is determined by many factors, such as government regulations, proximity of nearby transmitting stations and local geography. It is therefore usually necessary to *synthesize* the required frequency by electronically multiplying a standard frequency supplied by an atomic frequency standard. Frequency synthesizers linking the optical and microwave/RF regions are still at an early stage of development and are not commercially available, whereas such devices operating in the microwave region and lower frequencies are readily available.

Consequently, advances in trapped-atom and trapped-ion frequency standard technology have so far concentrated mainly on the microwave/RF region, and are the subject of this review.

Nevertheless, there have been some exciting recent advances in the observation of spectrally narrow optical resonances and precision optical metrology in trapped ions (see, for example Peik *et al* 1995, Barwood *et al* 1995, Bergquist *et al* 1991, Helmcke 1996). These advances, in conjunction with the inevitable development of compact, reliable and cost-effective microwave–optical and optical–optical frequency synthesizers will lead to extremely stable optical atomic frequency standards which may eventually revolutionize frequency metrology. This topic will no doubt be the subject of a future review.

For background reading, the subject and history of atomic frequency standards has been elegantly introduced in several papers and short reviews (see, for example, Itano and Ramsey 1993, Ramsey 1991, 1983, Lewis 1991, Dorenwendt and Fischer 1996).

The present review begins with a basic discussion of how atomic microwave frequency standards work, and some of the factors which limit their performance. In section 2 the performance characterization of frequency standards is introduced, and the theoretical performance limits of trapped-atom and trapped-ion frequency standards are discussed. In section 3 an overview of the principles and practices of trapped-ion standards is given, using the early $^{199}Hg^{+}$ standards as examples, and section 4 introduces the important problem of determining the frequency offsets caused by the environment of the trapped atoms or ions. In sections 5–9 all trapped-ion microwave frequency standards for which frequency stability data have been published are discussed individually. Section 10 discusses the Observatoire de Paris Cs fountain frequency standard, which at the time of writing is still the only operating trapped-atom frequency standard, although several other Cs fountain standards are under construction. Finally, the review concludes in sections 11 and 12 with a discussion of the critical problem of the limitations introduced by conventional local oscillators (LO).

1.1. Operation of atomic frequency standards

Figure 1 shows a block diagram of a generic passive atomic frequency standard. The system is termed passive because the reference atoms are interrogated by electromagnetic radiation,

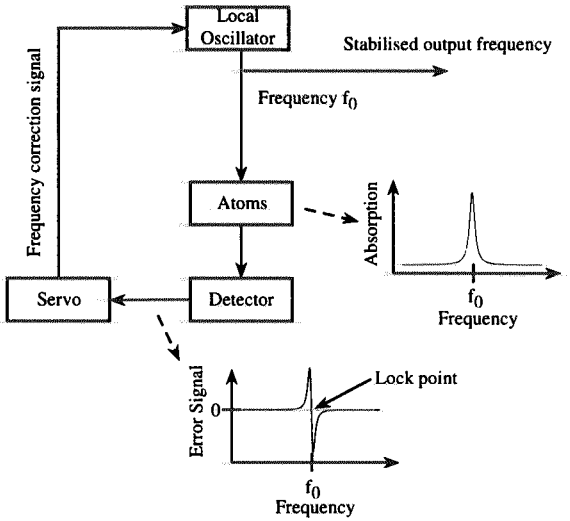

Figure 1. Schematic diagram of a generic passive atomic frequency standard. The purpose of the system is to maintain the frequency of the LO at the centre of the absorption resonance f_0 of an ensemble of atoms. The absorption resonance is generally symmetric about f_0, so that a deviation in LO frequency above or below f_0 cannot be directly distinguished. The detection system therefore generates the frequency derivative of the absorption signal and feeds this to the servo, which maintains the frequency of the LO at the zero-crossing (the 'lock point') of the error signal.

unlike *active* standards, such as most hydrogen masers, in which the atoms emit radiation. The detector monitors the degree to which the output of the LO is absorbed by the atoms, and the servo electronics maintain the frequency at the centre of the absorption resonance f_0. For optimum performance of the frequency standard, criteria which the absorption resonance should ideally satisfy include:

(a) The centre frequency f_0 of the resonance should be stable and as insensitive as possible to external influences, such as ambient magnetic and electric fields.

(b) The signal-to-noise ratio (SNR) of the absorption measurement should be as high as possible, to minimize the translation, by the servo electronics, of measurement noise into frequency noise.

(c) The full width at half-maximum (FWHM) Δf of the absorption resonance should be as small as possible, to enable the LO frequency to be stabilized to the centre frequency f_0 of the resonance with minimum influence of measurement noise.

(d) The centre frequency f_0 of the resonance should be as high as possible, consistent with the availability and practicality of frequency synthesizers suitable for converting the frequency f_0 to the frequencies required in the application of the standard.

The reasoning behind criterion (a) above is obvious. Criteria (b), (c) and (d) are linked by physical principles, to be discussed in this and the following sections, which are crucial to the motivation for developing trapped atom and trapped ion frequency standards.

The reason for criterion (b) is illustrated in figure 2. The servo 'sees' the noise on the absorption signal as instability in the frequency corresponding to its peak. Consequently, the servo system imposes the noise on the frequency of the LO as it attempts to track the apparently moving peak of the absorption resonance.

All real signals, electronic and otherwise, have a certain amount of noise superimposed

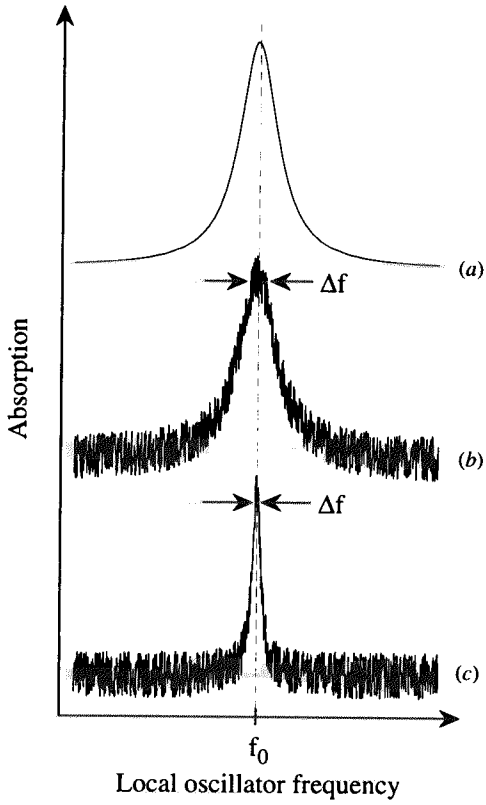

Figure 2. Illustration of the effect of noise on the absorption signal. (*a*) The ideal case, with no noise. The frequency corresponding to the peak of the error signal can be determined with no uncertainty. (*b*) Noise on the error signal introduces an uncertainty Δf in the frequency corresponding to the centre of the absorption resonance. (*c*) If the resonance is narrower, the same level of noise results in a smaller uncertainty in the position of the peak.

on them. This noise can arise from many sources, some of which can be eliminated or made insignificant by careful design, and others which are fundamental and cannot in practice be entirely eliminated. An example of a fundamental noise source arises from the quantization of electromagnetic radiation into photons, so that the total energy per unit time output by, for example, an incandescent lamp, is not smooth, but consists of a series of 'lumps' corresponding to the emission of each photon. When this light is converted into an electric current by a photodetector, in addition to other noise signals, the electric current typically also exhibits fluctuations with a 'white' frequency spectrum. This white noise, known as *shot noise*, or *quantum noise*, results from the quantization into photons of the energy emitted by the lamp, and from intrinsic statistical fluctuations in the photon arrival rate at the photodetector. Analogous noise arises from the process of counting the fraction of atoms which have absorbed a microwave photon during the measurement of the absorption profile of the atoms as shown in figure 1†. In this case, the number of atoms per unit time arriving at a detector is being measured, and the resulting noise often also exhibits a white frequency spectrum, identical to that of shot noise.

The level of development of commercial microwave atomic frequency standards is presently such that the short-term noise properties of the absorption signals are generally determined by fundamental processes such as those mentioned above. Consequently, a

† This can be understood by considering the hypothetical case where a single atom is used as a frequency reference. In order to observe a smooth absorption profile like that shown in figure 1, several measurements of each point on the profile must be made in order to average out the noise introduced by the fact that each measurement can have one of only two outcomes—the atom either does or does not absorb a microwave photon.

promising route to major improvements in stability is to reduce the spectral width of the absorption signal (figure 2(*c*)), and so reduce the degree to which absorption signal noise is translated into frequency noise in the LO by the servo. To understand the factors influencing the width of the absorption resonance, it is first necessary to discuss the basic physics of microwave absorption in atoms.

1.2. Microwave atomic absorption resonances

The requirements of radiofrequency and microwave atomic frequency standards, particularly criteria (a) and (c) mentioned in section 1.1, are best satisfied by a nuclear magnetic resonance (NMR) transition in the ground electronic state of certain atoms.

NMR occurs when the electromagnetic radiation incident on an atom is absorbed by the process of rotating the magnetic moment of the nucleus with respect to the net magnetic moment of the orbiting electrons. The simplest example of an NMR transition is an atom with nuclear spin quantum number $I = \frac{1}{2}$ and a single unpaired electron in the ground state, giving an angular momentum quantum number $J = \frac{1}{2}$ (figure 3). The total angular momentum F is given by

$$\begin{aligned} F &= J + I \\ &= 0 \text{ or } 1 \end{aligned} \tag{1}$$

where the quantum mechanical rules for the addition of angular momentum have been followed. The $F = 0$ state and the $F = 1$ state are separated in energy by the amount of energy W required to rotate the magnetic moment of the nucleus from an antiparallel to a parallel orientation. This energy separation is often referred to as *hyperfine splitting*, and transitions between these levels are often known as *hyperfine transitions*. The $F = 0$ and $F = 1$ states exhibit a magnetic dipole moment, so that a photon of electromagnetic radiation may be absorbed or emitted such that the hyperfine transition may occur while conserving energy, and the frequency f_0 (in Hz) of the photon is given by the familiar

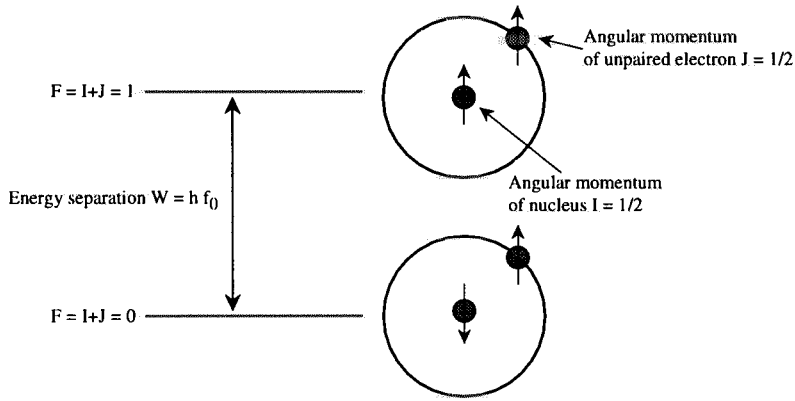

Figure 3. Energy-level structure of the ground electronic state of an atom with nuclear angular momentum quantum number $I = \frac{1}{2}$ and a single unpaired electron, giving a net electronic angular quantum number $J = \frac{1}{2}$. The two quantum-mechanically allowed relative orientations (parallel and antiparallel) of the angular momenta, and consequently the magnetic moments, yield a pair of states with total angular momentum quantum number $F = 0$ and 1. The energy separation of the levels due to this coupling between the nuclear and electronic angular momenta is also known as hyperfine splitting, or hyperfine structure.

relation

$$f_0 = W/h \tag{2}$$

where h is Planck's constant. An ensemble of such atoms prepared in the $F = 0$ state will therefore exhibit an absorption spectrum qualitatively similar to that shown in figure 2.

The transitions between atomic states used as frequency references in atomic frequency standards are often known as *clock transitions*.

We must now consider the factors which determine the FWHM of the absorption resonance, since, as shown in the previous section, this is a critical parameter for an atomic frequency standard. The Heisenberg uncertainty principle relates the uncertainty ΔE in the energy of a conservative system to a time interval t characteristic of the rate of change of the system;

$$\Delta E \tau \geqslant \frac{h}{2\pi}. \tag{3}$$

In the case of an atomic state, τ is clearly identifiable with the lifetime of the state.

Using

$$\Delta E = h \Delta f \tag{4}$$

gives the lower limit on the width, in frequency units, of the transition between the states $F = 0$ and $F = 1$:

$$\Delta f \geqslant \frac{1}{2\pi}\left(\frac{1}{\tau_{F=0}} + \frac{1}{\tau_{F=0}}\right). \tag{5}$$

Thus with no additional level broadening, the width of the absorption resonance is proportional to the sum of the reciprocal lifetimes of the two states. This immediately illustrates the advantage of choosing a NMR transition in the ground electronic state of an atom as a frequency reference, since spontaneous transitions out of these very low energy states are extremely unlikely, so that typical lifetimes extend to days and beyond, making absorption profile widths of a very small fraction of 1 Hz possible in principle. However, in order to realize the limiting absorption profile width given by equation (5), during the measurement of each point on the profile it is necessary to illuminate the atom with the near-resonant radiation for a time interval Δt_m which is longer than the lifetime of the levels. Because of the typically long lifetimes of the levels involved, this condition is very difficult to satisfy in practice. Consequently, the practical lower limit on the width of the absorption profile is generally the effective spectral width of the interrogating radiation source.

For example, an atom which is exposed to a monochromatic radiation source of frequency f_0 for an interrogation period Δt_m 'sees' a truncated sinusoidal waveform (figure 4). The effective spectral power profile $p_s(f)$ of the radiation is obtained from the Fourier transform of the truncated waveform;

$$\begin{aligned} p_s(f) &= \frac{2}{\pi}\left(\int_0^{N/2f_0} \sin 2\pi f_0 t \sin 2\pi f t \, \mathrm{d}t\right)^2 \\ &\approx \frac{2}{\pi}\left(\frac{\sin\left[(f_0 - f)\left(\frac{N}{2f_0}\right)\right]}{2(f_0 - f)}\right)^2 \qquad f_0 \gg 1 \text{ Hz and } f \approx f_0 \end{aligned} \tag{6}$$

where $N = \Delta t_m f_0$ is the number of cycles of the waveform occurring in the time interval Δt_m. The FWHM of the central peak of the power spectrum is

$$\Delta f \approx \frac{0.886}{\Delta t_m}. \tag{7}$$

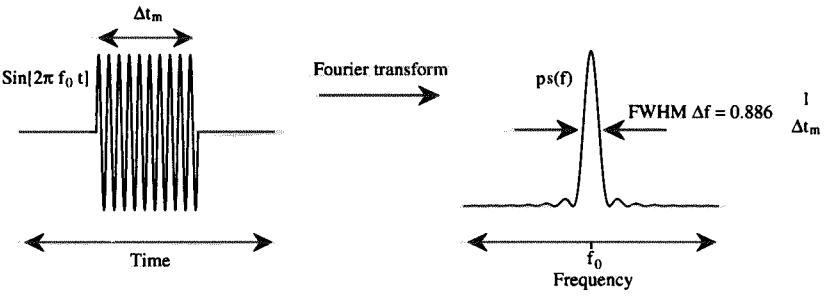

Figure 4. Microwave pulse of duration Δt_m (left) and corresponding power spectrum (right) showing the increase in effective spectral width due to the truncation of the waveform. All frequency units are Hz.

The numerator of equation (7) is specific to the case shown in figure 4, where the sinusoidal waveform of the incident radiation is modulated by a rectangular step function. However, in the more general case with an arbitrary modulating function, it is still generally true that,

$$\Delta f \approx \frac{1}{\Delta t_m} \tag{8}$$

where Δt_m characterizes the time over which the clock transition is interrogated.

Comparison of equations (8) and (5) shows that unless the time Δt_m, during which the atoms are exposed to the near-resonant interrogating radiation, significantly exceeds the lifetimes (often longer than one day) of the levels involved in the transition, the spectral width of the absorption profile will be dominated by the effective spectral width of the radiation source. This, then, is the primary motivation for the use of trapped atoms or trapped ions as an atomic frequency reference, since with these technologies it becomes possible to interrogate the atoms or ions over periods of several seconds or longer, thus achieving very high spectral resolution and consequently maximum suppression of the effects of noise in the atomic absorption signal. Finally, equation (8) also shows that the spectral width Δf of the microwave signal is independent of the centre frequency, so that for a given interrogation period Δt_m, the fractional spectral resolution $\Delta f/f$ (the inverse of this quantity, $f/\Delta f$, is known as the *Q factor*) improves with increasing centre frequency. This is the reason for criterion (d) of section 1.1.

1.3. The caesium standard

Because the ground-state hyperfine transition in ^{133}Cs atoms defines the SI second (see table 1), properly designed caesium atomic-beam microwave frequency standards (for brevity, hereafter referred to as caesium standards), generally do not require calibration in order to operate within their specified limits of accuracy. Consequently, the caesium standard is the most widely used microwave frequency standard in major calibration laboratories. The performance and limitations of modern caesium standards, including commercially available units as well as specially constructed laboratory units, are probably the benchmarks against which advances in microwave frequency standard technology will be judged. It is therefore worthwhile to introduce this topic in this review (for further details on caesium and other conventional atomic frequency standards see, for example, Vanier and Audoin (1989), Ramsey (1991), Lewis (1991) and Dorenwendt and Fischer (1996)).

The caesium standard, shown schematically in figure 5, operates by stabilizing a microwave frequency source at 9.2 GHz to the NMR transition between the $F = 3$ and

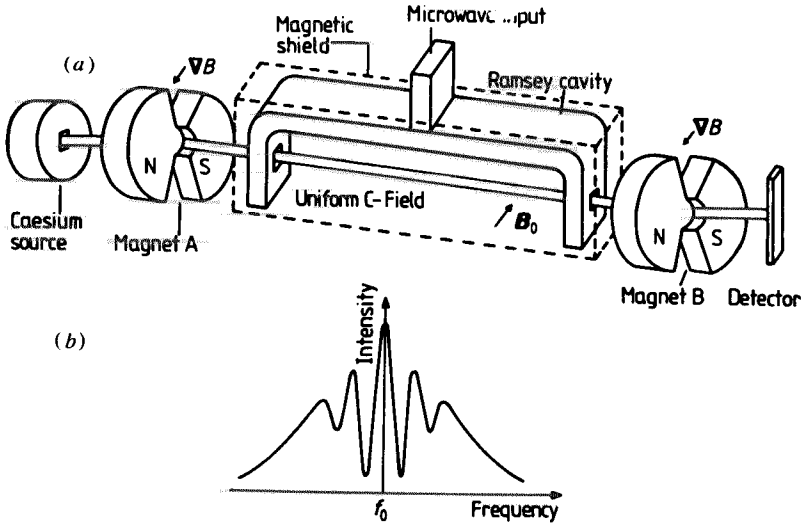

Figure 5. (*a*) The so-called 'physics package' of a Cs standard—see text. (*b*) The signal at the detector (rate of arrival of atoms) as a function of the frequency of the radiation applied to the Ramsey cavity. In commercially available Cs standards, the FWHM of the central peak is typically a few hundred Hz. From Vanier and Audoin (1989).

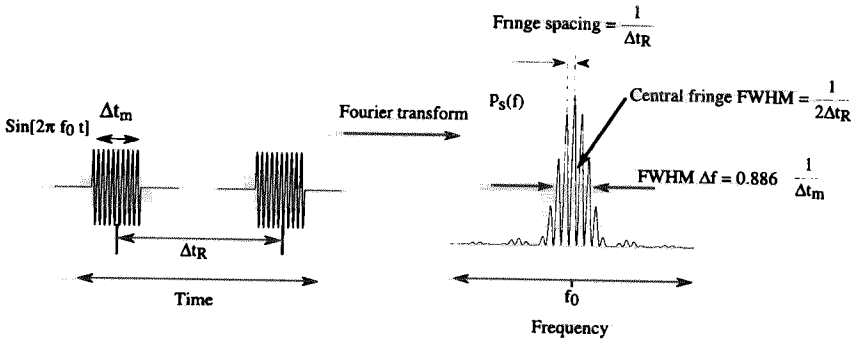

Figure 6. Microwave pulse sequence (left) and corresponding power spectrum (right) of microwave radiation 'seen' by a Cs atom as it passes through the two arms of the Ramsey cavity, in the limit where $\Delta t_R \gg \Delta t_m$ (cf figure 4). All frequency units are Hz.

$F = 4$ hyperfine levels of the electronic ground state of atomic ^{133}Cs. The atoms are emitted from an oven and are collimated into a beam, with a root mean square (RMS) speed of approximately 250 m s^{-1}. A state-selecting magnet permits only those atoms which happen to emerge from the oven in the $F = 3$ hyperfine level to pass through an aperture leading to the Ramsey waveguide cavity. Atoms in other states are deflected such that they do not pass through the aperture. The Ramsey waveguide cavity is designed such that the 9.2 GHz microwave radiation is confined as a standing wave within the two arms of the cavity, so that the atoms 'see' two well-defined pulses of radiation (figure 6) as they pass through apertures in each arm. In commercially available units, the two arms of the Ramsey cavity are typically separated by approximately 15 cm, so that for a typical atom the pulses are separated by a time interval Δt_R of approximately 1 ms. Atoms which emerge

from the downstream arm of the cavity having interacted resonantly with the microwave radiation and undergone a transition to the $F = 4$ state are selected by a second magnet, and are detected. A typical signal from the detector, as a function of the frequency of the microwave radiation, is shown in figure 5(*b*). The signal, known as a Ramsey pattern (see, for example, Vanier and Audoin 1989, chapter 5) consists of a series of 'fringes' (Ramsey fringes) separated in frequency by $(\Delta t_R)^{-1}$ on a wider background 'pedestal'.

As in the simpler single-pulse sequence considered in section 1.2, the form of the Ramsey fringes is determined by the effective spectral width of the microwave radiation, as seen by the atoms passing through the Ramsey cavity. Taking the Fourier transform (figure 6) of the double-pulse sequence experienced by the Cs atoms gives a spectrum consisting of sinusoidal fringes with FWHM $= (2\Delta t_R)^{-1}$ separated by $(\Delta t_R)^{-1}$, within a sinc function envelope given by the Fourier transform of a single pulse (figure 4)†.

In practice, the thermal atomic beam consists of atoms with a significant range of velocities. The actual spectrum (figure 5(*b*)) therefore consists of contributions corresponding to a range of pulse separations Δt_R, which causes a loss of fringe visibility towards the edges of the spectrum.

The Ramsey pattern $S(f)$ is, in principle, symmetric about the central frequency f_0. If the interrogating microwave radiation of frequency f is initially tuned to the central frequency f_0 and subsequently drifts in frequency, observing $S(f)$ will enable the magnitude of the drift to be calculated, but not the direction of drift. A signal, known as the error signal, which contains information on both the magnitude and direction of drift must obviously be supplied to the servo system (figure 1) which locks the interrogating radiation frequency to f_0. The frequency derivative of $S(f)$ (figure 7) satisfies the above requirements, since it changes sign as f passes through f_0. In practice, by modulating the phase or frequency of the interrogating radiation it is relatively simple (see, for example, Vanier and Audoin 1989) to generate the frequency derivative of $S(f)$, and for the purposes of further discussion we will call this derivative the error signal $E(f)$;

$$E(f) = \frac{\mathrm{d}}{\mathrm{d}f} S(f). \tag{9}$$

The servo system adjusts the LO frequency f to maintain the error signal $E(f)$ at the point, known as the lock point, where it crosses zero at f_0.

The noise characteristics of the reference signal $S(f)$, and the electronic components which subsequently process it, affect the precision with which the servo system can maintain f at the lock point, as illustrated in figure 7(*a*). Fluctuations in $S(f)$ appear on the error signal $E(f)$, and cause an uncertainty Δf in the frequency at which the error signal crosses zero. The servo system cannot therefore maintain f at f_0 with a precision better than Δf, and f therefore fluctuates within a range $\pm\Delta f/2$ around f_0. However, as mentioned in section 1.3 and shown in figure 7(*b*), by decreasing the FWHM of the Ramsey fringes, the magnitude Δf of the resulting frequency fluctuations can be reduced due to the greater slope of the error signal as it crosses the lock point f_0.

It is therefore desirable to decrease the width of the central Ramsey fringe, by increasing the interaction time Δt_R either by obtaining slower atoms from a thermal atomic beam (see, for example, Bauch *et al* 1993a), or by extending the distance between the arms of the

† In this and the previous section it has been implicitly assumed that the shape of the experimentally measured absorption resonance is given by the spectral shape of the interrogating radiation as seen by the reference atoms. Due to the quantum nature of the interaction between electromagnetic radiation and atoms, this is only true under certain conditions (e.g. microwave intensity and pulse length). However, most atomic frequency standards, including those discussed in this review, are configured so that these conditions are satisfied. For further reading, see, for example, Cohen-Tannoudji *et al* (1992) and Allen and Eberly (1975).

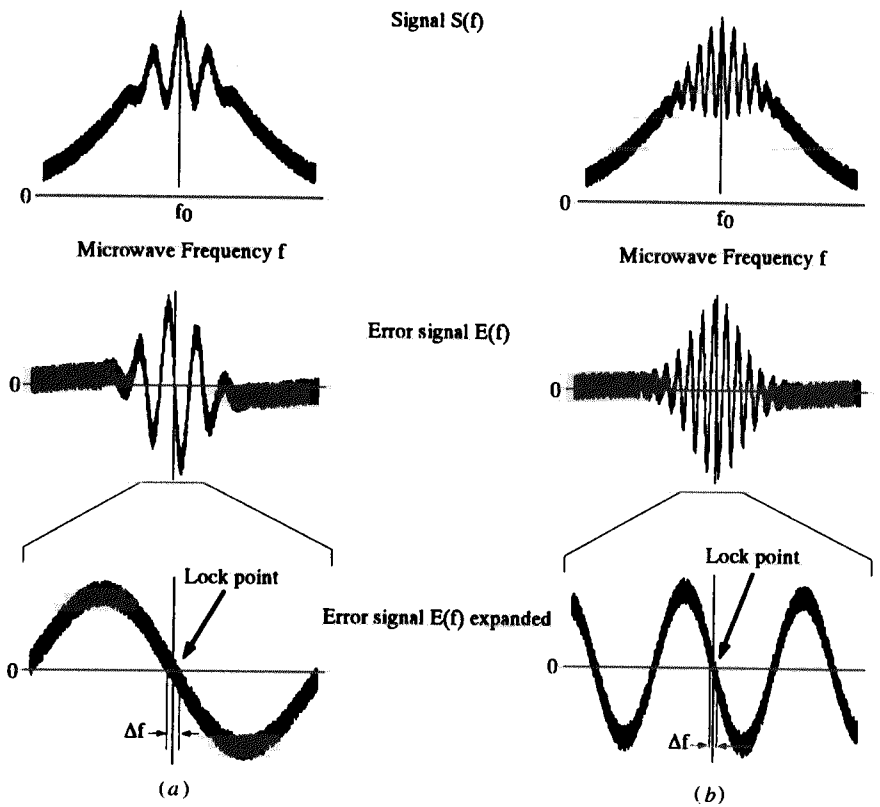

Figure 7. (*a*) and (*b*) Simulated reference signals $S(f)$ and corresponding error signals $E(f)$ with equal amounts of noise added. The FWHM of the Ramsey fringes in (*b*) is 2.5 times less than those in (*a*), and the resulting uncertainty Δf in the frequency of the lock point is correspondingly smaller.

Ramsey cavity (see, for example, Bauch *et al* 1988). There are clear practical limitations to both of these approaches, and interaction times Δt_R of more than a few tens of milliseconds, corresponding to Ramsey cavities with arms separated by several metres, are very difficult to realize.

The motivation for the development of atom and ion trapping technology for frequency standards purposes is again clear, since this technology provides solutions to the problem of substantially extending the atomic interrogation times.

2. Characterization of frequency noise and stability

It is important to distinguish between the *stability* and the *accuracy* of a frequency standard. As mentioned in section 1.1, the performance of any oscillator or any frequency standard is affected to some extent by many noise sources, including statistical noise in detection processes, electronic noise, vibration and thermal drifts. These factors often manifest themselves as instability in the frequency output of the standard, which means that if the output is observed over a period of time, some variation will be evident. A frequency standard's stability is therefore determined by how offsets affecting the frequency of its output vary in time. The *accuracy* of a frequency standard reflects, on the other hand, the

uncertainty within which the magnitude and sign of these frequency offsets is known. In the context of an atomic frequency standard, the term 'frequency offset' generally means the frequency perturbations on the clock frequency of the reference atoms induced by factors such as magnetic fields, electric fields and atomic motion, which are inherent to a particular design of frequency standard.

The rubidium microwave frequency standard (see, for example, Vanier and Audoin 1989) is a good example of a frequency standard which has good stability but relatively poor accuracy. This means that although its frequency offsets are relatively unknown, and vary from unit to unit, they are well controlled and remain reasonably constant. In practice, once a rubidium standard is calibrated by comparison with a more acccurate standard, its frequency remains constant to within a known tolerance for a usefully long time, typically six months or longer. On the other hand, modern commercially available caesium standards are typically accurate to within a few parts in 10^{12} or better, and when operating correctly will therefore indefinitely maintain their output frequency to within this tolerance of the SI definition, without initial or recurrent calibration. Of course, in return for this extra capability, a caesium standard usually costs much more to purchase and maintain than a rubidium standard.

Both the accuracy and stability of a frequency standard are therefore important quantities when making a decision on which type of frequency standard best suits a given application, and also when evaluating the potential usefulness of new designs of atomic frequency standards. In this section we consider how stability may be characterized, leaving the determination of accuracy to be discussed in section 4.

2.1. The Allan variance

If the output frequency f_1, averaged over a time interval τ, of a frequency standard is repeatedly measured, for example using the technique shown in figure 8, the result will be a time-series of fluctuating frequency readings. It is easy to see that plotting the amplitude of the fluctuations in the frequency readings against the time scale over which they occur may be very useful for characterizing and identifying their source; for example, thermal drift effects might be expected to produce frequency fluctuations over a much longer time scale than those caused by vibration. A great deal of theoretical effort has been applied to analyses of this type, and the most commonly used is known as the Allan deviation $\sigma_y(\tau)$, given by (Allan 1987)

$$\sigma_y(\tau) = \sqrt{\langle \tfrac{1}{2}(y(t+\tau) - y(t))^2 \rangle} \tag{10}$$

where the angular brackets denote an infinite time average, and

$$y(t) = \frac{f_1(t) - f_0}{f_0}. \tag{11}$$

Here, f_0 is assumed to be sufficiently more stable than f_1 so that its fluctuations may be neglected.

In practice, $\sigma_y(\tau)$ may be calculated from a series of M frequency measurements f_{1i} using

$$\sigma_y(\tau) \approx \left(\frac{1}{2(M-1)} \sum_{i=1}^{M-1} (y_{i+1} - y_i)^2 \right)^{\frac{1}{2}} \tag{12}$$

where

$$y_i = \frac{f_{1i} - f_0}{f_0}. \tag{13}$$

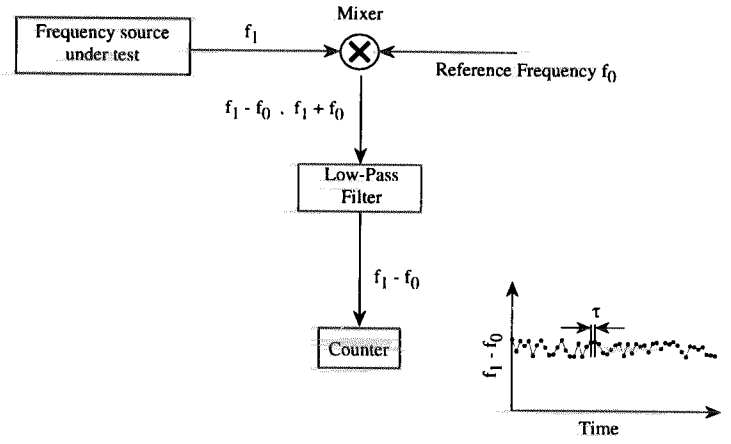

Figure 8. One method for measuring the frequency stability of a source by comparison with a much more stable reference frequency f_0. The two frequencies f_1 and f_0, typically in the RF (10^6 Hz) or microwave (10^{10} Hz) region are typically chosen to be very close, so that the difference frequency $f_1 - f_0$ recorded by the counter is of the order of a few hundred Hz or less. In this way, even a relatively inexpensive counter with 0.001 Hz resolution can measure frequency differences of parts in 10^{13}. The counter outputs the average value of $f_1 - f_0$ over a time interval τ every τ seconds, where τ is its gate time.

In equation (12), the approximation becomes exact as $M \to \infty$. For the case where y_i is defined according to equation (13), that is, where the nominal frequency f_0 of the standard is divided out, $\sigma_y(\tau)$ and $(\sigma_y(\tau))^2$ are commonly referred to as the *fractional Allan deviation* and *fractional Allan variance* respectively.

A plot of $\sigma_y(\tau)$ against τ represents a quantity analogous to the standard deviation of the fractional frequency fluctuations as a function of the time over which they are averaged. The performance, as characterized by the Allan deviation, of a number of commercial frequency standards as well as some of the trapped-atom and trapped-ion standards discussed in this review is shown in figure 9. On such a plot, noise arising from different physical processes has, in many cases, a characteristic signature. For example, quartz oscillators, which are often affected by thermal and other relatively slow drifts, generally exhibit large frequency fluctuations or drifts over long time scales (low frequencies), and smaller fluctuations over short time scales (high frequencies). Consequently, the Allan deviation of such an oscillator typically increases with averaging time (figure 9). Signals exhibiting white noise, where fluctuations occur with equal magnitude at all frequencies, are characteristic of measurements of quantities which fluctuate according to Poisson statistics. Such signals are usually obtained from counting type measurements, for example the arrival rates of photons from a source of constant power, or atoms from an atomic beam of constant average flux, at a detector. In the caesium standard, the white noise in the atom arrival rate appears on the error signal, and is translated into white frequency noise by the servo electronics. Since an important feature of signals exhibiting white noise is that their fluctuations decrease with the square root of the time over which they are averaged, this noise appears on a log–log Allan deviation plot as a line of slope $-\frac{1}{2}$ (figure 9). Thus in the case of white frequency noise, the longer the frequency is averaged, the more precisely it is determined.

The output of a given frequency standard typically exhibits two or more types of noise, depending on the averaging time τ, with different noise types being dominant at different averaging times. For example, the rubidium standard often exhibits (figure 9) near-white

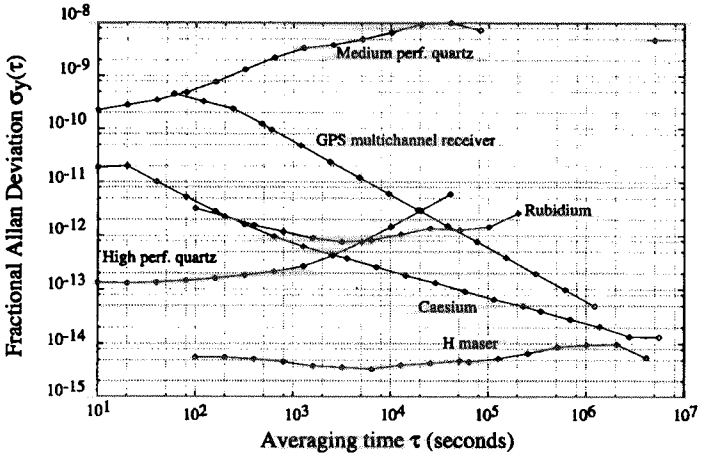

Figure 9. Fractional Allan deviation of several different types of frequency standards. The data shown was measured at the CSIRO National Measurement Laboratory, Australia. With the exception of the H maser, all units represented here are commercially available.

noise over short averaging times and drift characteristics over longer time scales. It is therefore not generally useful to compare the stability of two frequency standards without specifying the time interval over which their output frequencies are to be averaged. For this reason, a plot of the Allan deviation against averaging time has become the most common and generally the most useful measure of the overall stability of a frequency standard. For a far more complete discussion of the response of the Allan deviation to different types of noise, see, for example, Allan (1987) and Rutman and Walls (1991).

2.2. *Limiting Allan deviation for trapped-atom/ion standards*

Any passive atomic frequency standard must modulate the frequency of its LO in some way in order to locate the peak of the absorption profile of its atomic reference. This gives rise to the concept of a measurement cycle, which is the series of operations required to make a single measurement of the frequency difference between the LO and the atomic reference. A typical measurement cycle for a trapped-atom or trapped-ion† microwave frequency standard consists of measuring the signals S_+ and S_- obtained with the LO frequency shifted up and down by half the FWHM of the absorption signal or, as in the illustration presented in figure 10, one quarter of the Ramsey fringe separation δf_R (also see figure 6).

The frequency of the LO with respect to the peak of the central fringe is easily shown to be (for $f-f_0 \ll \delta f_R/4$—that is, for f near the peak of the central fringe)

$$f - f_0 \approx \frac{(S_- - S_+)}{S_0}\frac{\delta f_R}{2\pi}. \tag{14}$$

Inspection of equation (14) reveals that it has the desired property of an error signal in that it crosses zero at the lock point f_0.

The RMS fluctuations Δf_{RMS} in $f-f_0$ introduced by the RMS fluctuations $\Delta S_{\pm RMS}$ in

† Since most of what is presented in this section is applicable equally to trapped-atom or trapped-ion standards, for brevity, the term 'trapped-atom standards' will be used for both.

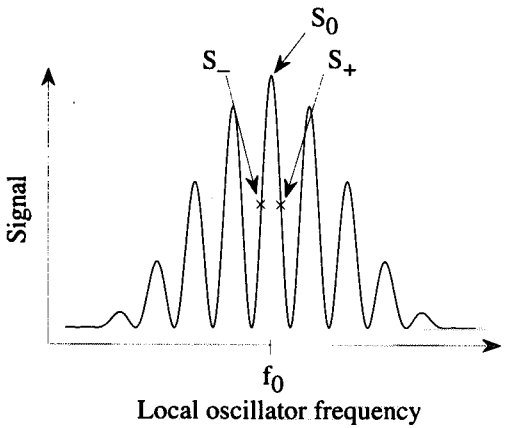

Figure 10. A simple method, commonly used in trapped-atom and trapped-ion standards, for locating the frequency corresponding to the peak of the central fringe of a Ramsey pattern. The signals obtained by shifting the LO frequency f up and down by $\delta f_R/4$, that is one quarter of a Ramsey fringe spacing, are recorded. If the two signals are equal, then the peak of the central fringe lies midway between them. If not, the frequency deviation $f-f_0$ is given by equation (14).

$S_\pm$ are (Wineland *et al* 1981, 1989):

$$\Delta f_{RMS} = \frac{\delta f_R}{2\pi} \frac{\sqrt{\Delta S^2_{+RMS} + \Delta S^2_{-RMS}}}{S_0}. \tag{15}$$

The measurement of S_+ and S_- fundamentally involves counting the number of atoms which have absorbed a microwave photon. For the case where $f \approx f_0$ the RMS fluctuations in $S_\pm$ have the statistical properties of shot noise or quantum noise, and follow a Poisson distribution (Wineland *et al* 1981), so that:

$$\Delta S_{\pm RMS} = \sqrt{S_\pm}. \tag{16}$$

Noting that when the LO frequency is close to the lock point $S_+ \approx S_- \approx S_0/2$, that $\delta f_R = \Delta t_R^{-1}$ (see figure 6) and that the time (the *measurement cycle time*) T_c required to make a single measurement of the error signal is at least $2\Delta t_R$ yields (Wineland *et al* 1981, 1989):

$$\sigma_y(\tau = 2\Delta t_R) = \frac{\Delta f_{RMS}}{\sqrt{2} f_0} = \frac{1}{2\sqrt{2}\pi f_0 \Delta t_R \sqrt{S_0}}. \tag{17}$$

Due to the property of the Poisson distribution expressed in equation (16), the fluctuations Δf_{RMS} averaged over k measurement cycles will decrease in magnitude proportionally to $k^{-1/2}$, which leads to the important result (noting that $k = \frac{\tau}{2\Delta t_R}$):

$$\begin{aligned} \sigma_y(\tau) &= \frac{1}{2\sqrt{2}\pi f_0 \Delta t_R \sqrt{S_0}} \sqrt{\frac{2\Delta t_R}{\tau}} \\ &= \frac{1}{2\pi f_0 \sqrt{\Delta t_R} \sqrt{S_0}} \sqrt{\frac{1}{\tau}}. \end{aligned} \tag{18}$$

Equation (18) is valid for the case where the fluctuations in the measured signals $S_\pm$ are due entirely to fluctuations in the number of atoms which have been excited by a microwave photon. This is equivalent to requiring that these excited atoms are detected with 100%

probability, so that no additional fluctuations are introduced by statistical variations in the detection process. In practice, it is possible to approach this ideal efficient detection regime (see, for example, Wineland *et al* 1981), and under these conditions S_0 in equation (18) may be replaced with the number n of atoms being interrogated by the microwave radiation:

$$\sigma_y(\tau) = \frac{1}{2\pi f_0 \sqrt{\Delta t_R n \tau}}. \tag{19}$$

Thus the stability performance of the trapped-atom standard improves with the inverse square root of the interrogation time Δt_R and the inverse square root of the number of atoms which are interrogated. The dependence on the inverse of the frequency f_0 of the standard is a strong motivation for the development of optical frequency standards.

Recognizing that the intrinsic SNR of the standard is given by

$$\text{SNR} = \frac{S_\pm}{\sqrt{S_\pm}} = \frac{n}{\sqrt{n}} \tag{20}$$

leads to a more physically enlightening form of equation (19):

$$\sigma_y(\tau) = \frac{1}{2\pi f_0 \text{SNR} \sqrt{\Delta t_R \tau}}. \tag{21}$$

Finally, in practice, the cycle time T_c required to make a single interrogation of the error signal is sometimes significantly longer than the theoretical minimum $2\Delta t_R$, in which case (Clairon *et al* 1995)

$$\sigma_y(\tau) = \frac{1}{2\pi f_0 \Delta t_R \text{SNR}} \sqrt{\frac{T_c}{\tau}} \frac{\sqrt{2}}{\sqrt{2}} \quad \tau \geqslant T_c \geqslant 2\Delta t_R. \tag{22}$$

It should be clearly understood that the performance analysis presented in this section is based purely on SNR considerations. There are of course other factors which determine the ultimate performance of a given frequency standard, that is, whether, and over what averaging times t, the performance of the standard achieves the performance limit given by equations (19) and (22). For example, it is unrealistic to expect the stability, characterized by $\sigma_y(\tau)$, to continue to improve proportionally to $\tau^{-1/2}$ without limit as the averaging time τ is increased. In practice, over a sufficiently long averaging time an instability due to some residual and uncompensated perturbation of the reference atoms will result in $\sigma_y(\tau)$ departing from the ideal $\tau^{-1/2}$ behaviour.

The limiting performance of a trapped-atom standard, calculated using equation (19), is shown in figure 11 for the single-atom optical case and the microwave case for a single atom and a cloud of 10^6 atoms. An interrogation time Δt_R of 20 s was assumed in each case. For an optical standard, the ideal case of a single isolated atom or ion offers stability performance (figure 11) potentially exceeding that of any present frequency standard, due to the f_0^{-1} dependence of equation (22) (i.e. the greatly increased Q factor of the interrogation signal). In contrast, the stability performance of a single-atom microwave standard cannot rival, at least over time scales of up to one day, the present state of the art in conventional caesium standards. Consequently, frequency standards based on clouds of trapped atoms or ions, despite the perturbations (to be discussed later in this review) which arise from their mutual interaction, remain of interest.

Nevertheless, a single atom or ion either suspended or in free fall in a perfect vacuum is perhaps the ideal atomic reference, since perturbations due to interactions with other atoms are absent. A microwave frequency standard based on a single atom or ion may therefore be a useful device even if long averaging times are required to realize its potential stability and accuracy.

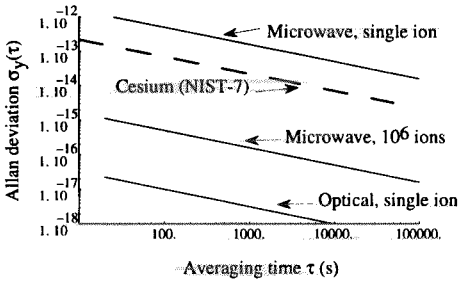

Figure 11. Comparison of the limiting performance of a trapped-atom/ion standard, calculated using equation (19), with the best reported performance from a conventional caesium standard (NIST-7) (Lee *et al* 1995). For the calculated performances, the microwave and optical frequencies were assumed to be 10^{10} Hz and 5×10^{14} Hz respectively, and the interaction time Δt_R was assumed to be 20 s.

It should be noted that the realization of a single-atom optical standard with the performance ($\sigma_y(\tau) = 10^{-16}\tau^{-1/2}$) shown in figure 11 would require an optical LO, possibly a laser, with a fractional stability over 20 s of $10^{-16}/\sqrt{20} = 2 \times 10^{-17}$. Lasers of such stability have not yet been demonstrated. The requirements imposed on LO by trapped-atom and trapped-ion frequency standards will be discussed further in section 11.

It is theoretically possible to obtain stability performance better than the limit given by equation (19) by preparing the ensemble of atoms in a non-classical state, known as a spin-squeezed state (Wineland *et al* 1992, 1994, Itano *et al* 1993). In spin-squeezed states the states of the individual atoms comprising the ensemble are not independent of each other, but are quantum-mechanically correlated. Under appropriate conditions, this results in the fluctuations in the number of atoms which have absorbed a microwave photon after interrogation being smaller than that predicted by Poisson statistics, which assumes that the atoms behave independently from one another. Improvements in SNR of approximately $n^{1/2}$ are predicted in certain cases, where n is the number of atoms in the ensemble.

Probing the atoms with electromagnetic radiation prepared in a non-classical 'squeezed' state has also been proposed as a technique for achieving sub-Poisson fluctuations in microwave absorption resonances (Batygin *et al* 1992). The application of either of the above two non-classical techniques to a prototype frequency standard has yet to be reported.

3. Introduction to trapped-ion frequency standards

The development of high-resolution microwave and radiofrequency spectroscopy of trapped ions has been discussed in several papers and reviews, and at least one specialized monograph (Itano 1991, Itano *et al* 1987, Paul 1990, Werth 1985, 1987, Wineland and Itano 1983, Drullinger *et al* 1996, Ghosh 1995). The coverage of trapped-ion spectroscopy in the present review will be restricted to work carried out specifically with a frequency standard application in mind. As a result, only two of the several different types of ion trap, the Paul trap and the Penning trap, need be covered here.

3.1. RF ion trapping

The outline of radiofrequency ion trapping presented in this section is a summary of an earlier and more detailed treatment (Dehmelt 1967, 1969). Consider a particle of mass

m and charge q, subjected to an electric field which oscillates sinusoidally with angular frequency Ω and amplitude E_0. The force $F(t)$ experienced by the particle is

$$F(t) = qE_0 \cos(\Omega t). \tag{23}$$

If the particle is initially at rest at $y = 0$, the steady-state time-dependent velocity $\dot{y}(t)$ and position of the particle $y(t)$ are given simply by

$$\begin{aligned} \dot{y}(t) &= \frac{qE_0}{m\Omega} \sin(\Omega t) \\ y(t) &= \frac{-qE_0}{m\Omega^2} \cos(\Omega t). \end{aligned} \tag{24}$$

Thus the particle oscillates sinusoidally, and its displacement is π out of phase with the force exerted by the driving electric field. The force and consequently the position of the particle averages to zero over one cycle of the oscillating electric field.

In the case where the oscillating field is spatially inhomogeneous (figure 12), equation (23) becomes

$$F(t) = qE_0(y) \cos(\Omega t). \tag{25}$$

For a sufficiently high oscillation frequency, the excursion $y - y_{av}$ from the average position y_{av} during one cycle of the driving field, will be small. This approximation is known as the *pseudopotential approximation* (Schubert *et al* 1990). In this case $F(t)$ may be written:

$$F(t) = qE_0(y_{av}) \cos(\Omega t) + q\frac{dE_0(y_{av})}{dy}(y - y_{av}) \cos(\Omega t). \tag{26}$$

Using equation (24) for $y - y_{av}$ gives;

$$F(t) = qE_0(y_{av}) \cos(\Omega t) - \frac{q^2 E_0}{m\Omega^2} \frac{dE_0(y_{av})}{dy} \cos^2(\Omega t). \tag{27}$$

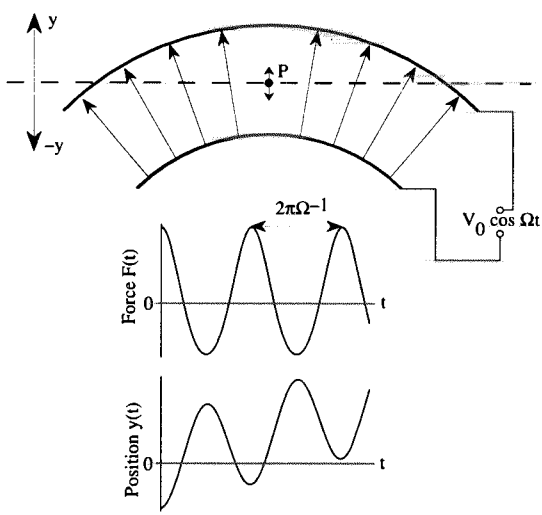

Figure 12. Illustration of the origin of the ponderomotive force experienced by a charged particle in an inhomogeneous oscillating electric field (after Dehmelt 1967).

Averaging equation (27) over one cycle of the oscillating electric field yields the *ponderomotive force*

$$F_{av}(y_{av}) = -\frac{q^2 E_0}{2m\Omega^2}\frac{dE_0(y_{av})}{dy} \tag{28}$$

which acts in the direction of decreasing amplitude of the oscillating electric field.

It can be seen from figure 12 that the ponderomotive force arises because the electrostatic force experienced by the particle during the positive and negative halves of the sinusoidal electric field cycle are no longer balanced, due to the motion, known as *micromotion*, of the particle at the RF frequency in the inhomogeneous RF electric field.

Extending equation (28) to three dimensions, and defining *the ponderomotive pseudopotential* $\Psi(x, y, z)$ by

$$F(\bar{x}, \bar{y}, \bar{z}) = -q\nabla\Psi(\bar{x}, \bar{y}, \bar{z}) \tag{29}$$

yields the result

$$\Psi(\bar{x}, \bar{y}, \bar{z}) = \frac{qE_0^2(\bar{x}, \bar{y}, \bar{z})}{4m\Omega^2} \tag{30}$$

where the bars over the spatial coordinates denote their average over one cycle of the oscillating electric field. An electric field which at some spatial point satisfies $\nabla\Psi = 0$ and $\nabla^2\Psi > 0$ is permitted by Maxwell's equations, and is capable of trapping positively or negatively charged particles or ions. Devices which use a combination of a DC potential and a ponderomotive pseudopotential for the confinement of ions, or in-principle, any charged particles, are known as Paul traps, or RF traps.

There are many configurations of electrodes and applied voltages which will work as a Paul trap; however, for many applications a pseudopotential which is harmonic and spherically symmetric is the most suitable for frequency standards purposes due to the simplicity of the resulting (simple harmonic) motion of the confined particles. Figure 13 shows a Paul trap whose electrodes are hyperboloids of revolution about the z-axis; this type of trap is commonly known as a *hyperbolic* Paul trap. For the case where the DC component U_0 of the oscillating potential applied to the electrodes is zero, the pseudopotential (in cylindrical coordinates r, z) is given by

$$\Psi(\bar{r}, \bar{z}) = \frac{qV_0^2}{m\Omega^2(r_0^2 + 2z_0^2)^2}(\bar{r}^2 + 4\bar{z}^2) \tag{31}$$

where the dimensions r_0 and z_0 are defined in figure 13. Appropriate† choice of the trap parameters V_0, Ω and the DC bias voltage U_0 yields a spherically symmetric harmonic pseudopotential proportional to $\bar{r}^2 + \bar{z}^2$. Under these conditions an ion or a spherical cloud of ions is confined in a region centred on the origin.

For frequency standards purposes, it is important to understand the motion of the ions in the trap, since this motion results in a temperature-dependent second-order Doppler shift (to be discussed in detail in section 4.2) in the clock frequency. Individual ions of finite temperature execute harmonic motion in the pseudopotential well at thermal velocities. This motion, known as *secular motion* or *macro motion*, is characterized by the *secular frequency* ω_s which is a property of the pseudopotential and is given by (in angular frequency units,

† For a hyperbolic trap of given dimensions and a given ion mass m, only values of Ω, V_0 and U_0 within certain ranges yield stable confinement. The stability of hyperbolic traps has been discussed many times (see, for example, Wineland and Itano 1983, Dehmelt 1967).

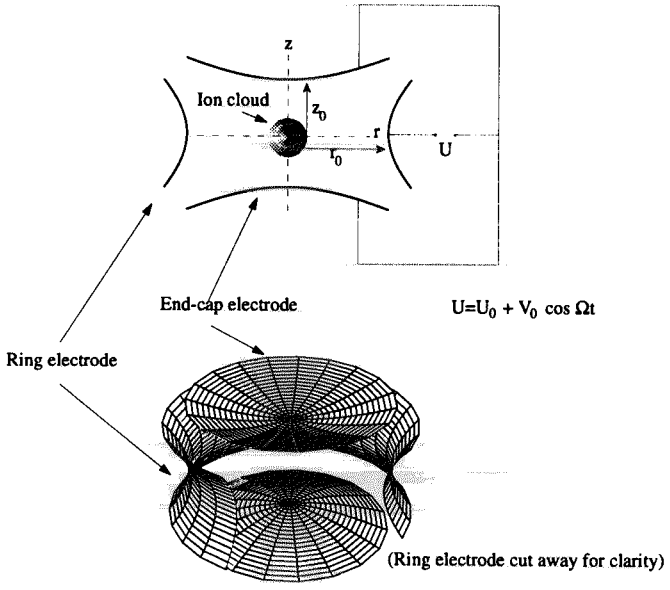

Figure 13. Schematic diagram of a hyperbolic Paul trap. The electrodes are normally housed in an ultra-high vacuum enclosure, since collisions with ambient gas molecules would otherwise tend to eject ions from the confining pseudopotential well.

and for the case where the potential is spherically symmetric (see, for example, Meis *et al* (1989) and Cutler *et al* (1986)):

$$\omega_s \approx \frac{2qV_0}{m\Omega(r_0^2 + 2z_0^2)}. \tag{32}$$

The motion of the trapped ions is complicated by the fact that when a significant number of ions are confined, an additional potential due to their mutual Coulomb repulsion must be added to the pseudopotential given by equation (31) to give the total confining potential. Thus equation (32) is truly valid only for a single trapped ion, or a low density of ions where the Coulomb potential is negligible compared with the pseudopotential. If this condition is not met, the observed secular frequency will be lower than that predicted by equation (32), and the discrepancy gives information (to be discussed in section 4.2) about the ion density. It is convenient to call the frequency ω_s, as given by equation (32), the *empty-trap secular frequency*.

At the geometric centre ($r = 0, z = 0$) of an ideal hyperbolic trap, the amplitude of the oscillating electric field is zero, and increases with distance from this point. Ions which are not at the centre of the trap therefore execute quasiharmonic micro-motion at the trap drive frequency Ω. The amplitude of this motion increases with distance from the centre of the trap.

An alternative configuration of the Paul trap which was first recognized as having certain advantages for frequency standards purposes by Prestage (Prestage *et al* 1988, 1989) is the linear trap shown in figure 14. In the linear trap the ions are confined in the two transverse directions by the RF pseudopotential alone, and a DC potential is used for confinement in the longitudinal direction. The extended nodal region of the RF field in the linear Paul trap is attractive for frequency standards purposes, and will be discussed in section 4.2.

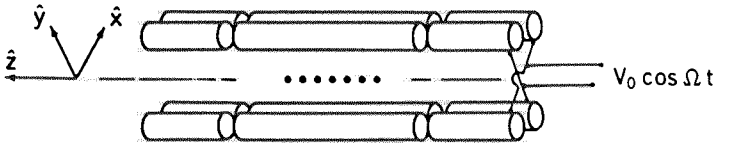

Figure 14. One configuration of a linear Paul trap. An alternating RF voltage $V_0 \cos \Omega t$ is applied to diagonally opposite electrodes as shown. The rod segments are capacitively coupled so that a DC potential may be applied to the end segments only, while maintaining the entire rods at the same RF potential. The DC potential prevents escape of the ions along the longitudinal axis of the trap (from Raizen *et al* 1992). Other linear Paul trap designs, which use separate DC end electrodes, have also been used in frequency standards work (e.g. Prestage *et al* 1989, Fisk *et al* 1995).

The Penning trap (see, for example, Paul 1990) has also been used for investigations of trapped ions as frequency standards, and is essentially the same as the hyperbolic Paul trap (figure 13), but with confinement in the radial direction provided by a magnetic field oriented parallel to the z-axis, rather than an oscillating electric field (i.e. $V_0 = 0$ in figure 13). The ions in such a trap execute a cyclotron motion around the z-axis.

Ion traps are often, but not always, loaded by evaporating atoms into the region between the trap electrodes, and ionizing the atoms with electrons emitted from a biased and heated filament.

3.2. Cooling of the trapped ions

One problem associated with the storage of large numbers of ions in Paul traps is that ion–ion collisions generally result in absorption of energy from the trapping RF electric field, and consequent heating of the ion cloud, sometimes to temperatures as high as 6000 K (Dehmelt 1967, 1969, Cutler *et al* 1985, 1987, Blümel *et al* 1989). This heating typically results in loss of ions from the trap as the more energetic ions escape from the potential well, and the heating effect increases with the size and density of the ion cloud. An additional effect of the resulting high ion cloud temperatures is an undesirably large offset in the measured clock frequency, due to the second-order Doppler shift. There are two obvious approaches which can be used to address these problems for frequency standards purposes. The first is to cool the ion cloud by introducing a light 'buffer' gas such as helium, at room temperature, into the vacuum system, to collisionally dissipate the thermal energy of the ion cloud (Lunney *et al* 1992). The second approach is to actively cool the ions close to 0 K using the momentum of photons of near resonant laser light (see, for example, Itano *et al* 1995). Trapped-ion frequency standards using both these approaches have been demonstrated, and will be discussed later in this review.

3.3. Early $^{199}Hg^+$ trapped-ion microwave frequency standards

In this section we introduce the detailed operational characteristics of trapped-ion microwave frequency standards (hereafter referred to as trapped-ion standards). We use as examples the first functional trapped-ion standards, based on $^{199}Hg^+$ confined in hyperbolic Paul traps, since the mode of operation of these systems is similar to most of the more recently developed systems. We will then discuss the Lamb–Dicke effect, which is crucial to the high spectroscopic resolution achievable in ion traps. Following this, the frequency offsets affecting the accuracy as well as the stability of trapped-ion standards will be discussed in

some detail, which will lead into the more recent frequency standards work using linear Paul traps. Armed with the above knowledge, the subsequent discussion of all the other reported work on trapped-ion and trapped-atom frequency standards should then be clear.

Studies of the first frequency standards based on trapped ions capable of continuous operation were reported separately by Jardino and co-workers of the Laboratoire de l'Horloge Atomiqe (Jardino and Desaintfuscien 1980, Jardino *et al* 1981b, Meis *et al* 1988, 1989) and by Cutler and co-workers of Hewlett-Packard. (Cutler *et al* 1981, 1983, 1985, 1986, 1987, Matsakis *et al* 1995). Both research groups developed standards (here labelled the LHA standard and the HP standard for convenience) based on the 40.5 GHz ground-state hyperfine resonance in $^{199}Hg^+$ confined in a hyperbolic Paul trap. Three $^{199}Hg^+$ HP standards have been in quasicontinuous operation since 1987 (Matsakis *et al* 1995), and the operating parameters of the standards discussed in this section are, unless otherwise stated, those corresponding to this long-term operation.

The configuration of the HP $^{199}Hg^+$ standards is shown in figure 15. The z_0 dimension of the trap (figure 13) was 1 cm. The ion trap was loaded by ionizing ^{199}Hg atoms, continuously introduced as a vapour into the vacuum system, by collisions with low-energy electrons emitted in pulses from a hot filament. The trap RF drive amplitude V_0 was about 150 V_{p-p} at 500 kHz, and a DC potential U_0 of 37 V yielded an approximately spherical pseudopotential well. The resultant empty-trap secular frequency ω_s (equation (32)) was $2\pi \times 50$ kHz. Helium was maintained in the vacuum system as a buffer gas at 1.3×10^{-3} Pa (Cutler *et al* 1987), and cooled the ion cloud close to 300 K.

$^{199}Hg^+$ (figure 16) has a ground-state hyperfine clock transition at 40.5 GHz. The

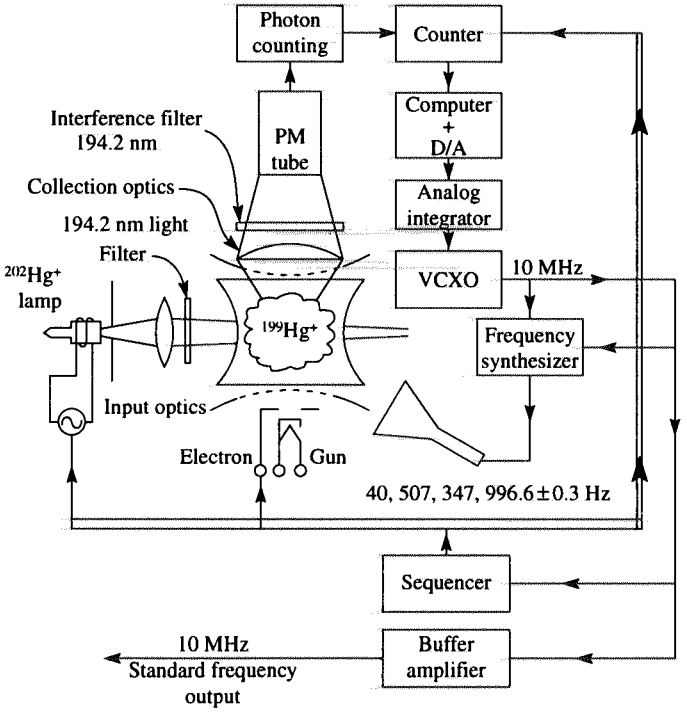

Figure 15. Schematic diagram of the HP 40.5 GHz $^{199}Hg^+$ microwave frequency standard. After Cutler *et al* (1981).

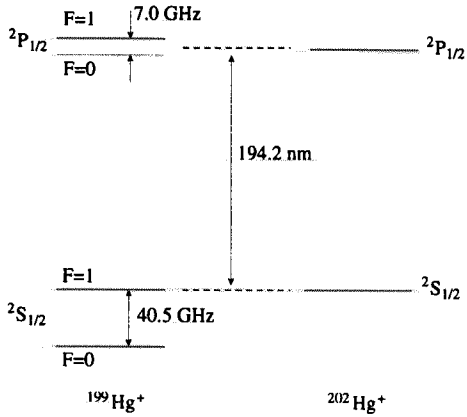

Figure 16. The simplified energy-level diagram for $^{199}Hg^+$ and $^{202}Hg^+$. Hyperfine structure is absent in $^{202}Hg^+$ as it has a nuclear spin quantum number $I = 0$.

standard operates by interrogating the ion cloud with 40.5 GHz microwave radiation and determining the precise microwave frequency at which the absorption of the interrogating radiation is maximized. Due to the mutual Coulomb repulsion of the ions, the density of the ion cloud is sufficiently low that only a very small fraction of the microwave photons will be absorbed. This makes it very difficult to measure the absorption directly by monitoring the power of the microwave radiation transmitted through the cloud. Instead, the $^{199}Hg^+$ standard uses a fortuitous coincidence (figure 16) between the frequencies of the optical resonance transition in $^{202}Hg^+$ and the $^2S_{1/2}F = 1 - {}^2P_{1/2}F = 0, 1$ transitions in $^{199}Hg^+$. Ultraviolet (UV) light at 194.2 nm from an RF-excited discharge lamp filled with $^{202}Hg^+$ illuminates the cloud of $^{199}Hg^+$ ions. The $^{199}Hg^+$ ions which happen to be excited to the $F = 1$ hyperfine component of the $^2S_{1/2}$ ground state will be further excited by the absorption of a UV photon to the $^2P_{1/2}F = 0$ or $F = 1$ state. After a few nanoseconds the ions will spontaneously decay back to the $F = 0$ or $F = 1$ component of the ground state, emitting a fluorescence photon in the process. If a $^{199}Hg^+$ ion decays back to the $F = 1$ component of the ground state the process will repeat itself, and another fluorescence photon will be emitted, however, if the ion decays to the $F = 0$ hyperfine component of the ground state, it will remain in that state, since there is no transition out of this state resonant with the light emitted by the $^{202}Hg^+$ lamp. Thus the entire population of $^{199}Hg^+$ ions will eventually be 'pumped' into the $F = 0$ component of the ground state, at which point interaction with the light from the $^{202}Hg^+$ lamp and the emission of fluorescence photons ceases.

This *optical pumping* process allows absorption of 40.5 GHz microwave photons by the $F = 0 \rightarrow F = 1$ ground-state hyperfine transition to be detected by monitoring the intensity of the 194.2 nm fluorescence emitted by the ions; for each microwave photon absorbed by a $^{199}Hg^+$ ion, one or more 194.2 nm fluorescence photons will be emitted, and can be detected and counted using, for example, a photomultiplier tube. The fluorescence signal can in principle be detected against a background of no optical photons, whereas the (very small) microwave absorption signal would need to be detected against the background power fluctuations in the microwave source.

The absorption lineshape of the 40.5 GHz clock transition in the trapped $^{199}Hg^+$ ions is shown in figure 17. Each point on the line was obtained by illuminating the ion cloud with a 'square' 0.24 s pulse of 40.5 GHz microwave radiation (figure 18), followed by

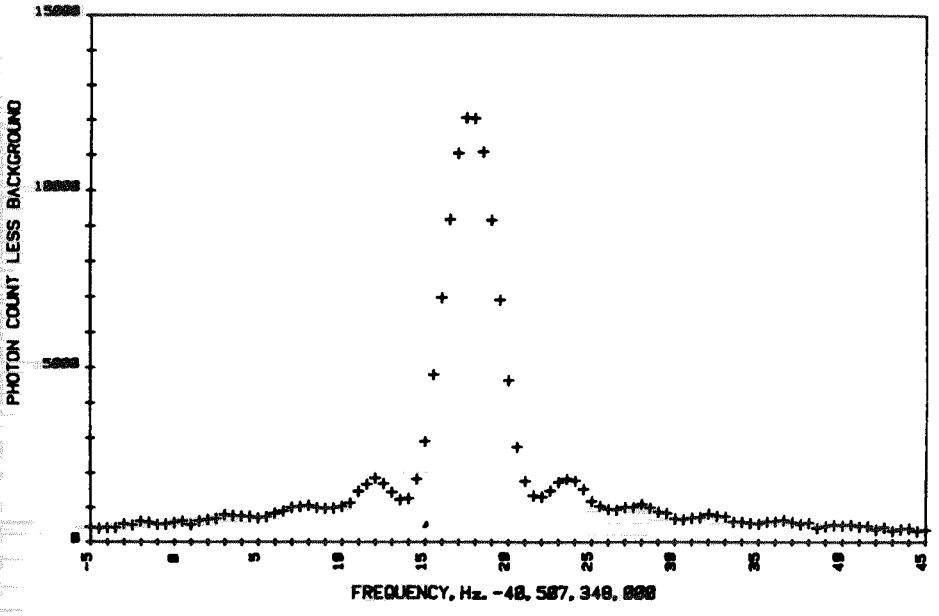

Figure 17. 40.5 GHz ground-state hyperfine absorption resonance of a cloud of approximately 2×10^6 $^{199}Hg^+$ ions (cf figure 1). The microwave pulse length was 0.24 s. The frequency has been corrected for the 10^{-5} T magnetic field, and the signal is the average of 60 sweeps. From Cutler *et al* 1981.

a pulse of 194.2 nm light from the discharge lamp. The reported signal is the number of 194.2 nm fluorescence photons recorded at each microwave frequency, with the background due to direct scatter of the lamp's output from internal surfaces of the ion trap subtracted. The FWHM of the signal, about 3.5 Hz, is in reasonable agreement with the microwave radiation's effective Fourier bandwidth, 3.7 Hz, predicted by equation (7) for the 0.24 s square microwave modulating pulse. The general form of the signal is also similar to that shown in figure 4, showing a broadening and sidebands due to the truncation of the microwave waveform.

In continuous operation, both the HP and LHA $^{199}Hg^+$ standards servo-lock the frequency of a quartz oscillator (multiplied to the 40.5 GHz clock frequency—see figures 1 and 15) to the centre of the resonance peak shown in figure 17. Measurements of the SNR of the hyperfine resonance indicate (Cutler *et al* 1981) a theoretical maximum stability performance characterized by a fractional Allan deviation $\sigma_y(\tau) = 1.2 \times 10^{-12}\tau^{-1/2}$ (see equation (21)) for averaging times τ longer than the servo time constant (about 20 s). Remarkably, nearly eight years of stability data is available from three HP standards (Matsakis *et al* 1995), and over a particular period of 268 days the fluctuations in the frequency difference between two of the units exhibited a fractional Allan deviation $\sigma_y(\tau) = 6.7 \times 10^{-15}$ over averaging times τ of 1 day (which is in good agreement with the theoretical performance), and $\sigma_y(\tau) = 4.7 \times 10^{-15}$ over 10 days. The LHA standard demonstrated a performance characterized by $\sigma_y(\tau) = 3.6 \times 10^{-11}\tau^{-1/2}$ for averaging times $10 \text{ s} < \tau < 3500$ s (Jardino *et al* 1981a, b).

For comparison, the published performances, as characterized by the Allan deviation, of all the trapped-atom/ion standards discussed in this review are plotted in figure 19.

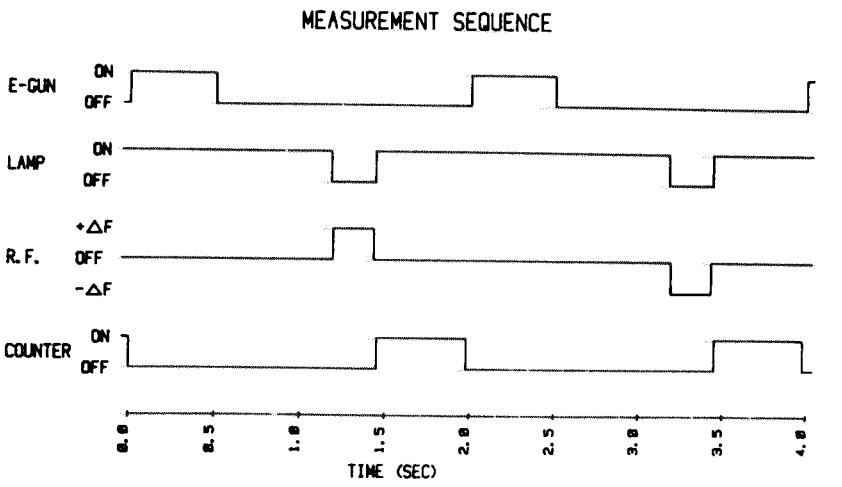

Figure 18. $^{199}Hg^+$ frequency standard measurement sequence. (1) The electron gun (E-GUN) loads the trap by ionizing ^{199}Hg atoms from a background vapour in the vacuum system. (2) The $^{202}Hg^+$ lamp is turned on to optically pump the trapped $^{199}Hg^+$ into the $F = 0$ hyperfine component of the ground state. (3) The trapped $^{199}Hg^+$ ions are illuminated by a microwave pulse (denoted R.F. in the figure). (4) The $^{202}Hg^+$ lamp is turned on again, and the fluorescence from ions excited by the microwave pulse to the $F = 1$ hyperfine component of the ground state is recorded. For locking of the microwave frequency to the centre of the peak shown in figure 17, the cycle was repeated with the microwave frequency shifted alternately up and down by one half of the FWHM δ_{FWHM} of the peak, and the error signal calculated using equation (14), with δf_R replaced by $2\delta_{FWHM}$. From Cutler *et al* (1981).

3.4. The Lamb–Dicke effect

A special feature of spectroscopy on trapped atoms or ions becomes apparent when we note that a hypothetical experiment to measure a corresponding line profile on $^{199}Hg^+$ ions which are not confined in a trap would yield a profile whose minimum FWHM Δf is determined by Doppler broadening (see, for example, Corney 1977, p 248);

$$\Delta f = \frac{2f_0}{c}\sqrt{\frac{2kT\ln 2}{m}} \tag{33}$$

where f_0 is the frequency corresponding to the centre of the profile, T is the temperature of the ion cloud and m is the mass of a single ion. Inserting $T = 300$ K into equation (33) yields an expected minimum FWHM (known as the Doppler width) of about 35 kHz for $^{199}Hg^+$, far in excess of that observed in the trapped ion cloud (see figure 17), which we would expect to be hotter†.

The absence of Doppler broadening in the spectrum shown in figure 17 is a manifestation of the Lamb–Dicke effect (Dicke 1953).

Perhaps the simplest way of understanding the Lamb–Dicke effect is to note that in our hypothetical unconfined gas of $^{199}Hg^+$ ions (or atoms), Doppler broadening arises from the fact that individual ions with a thermal velocity component v' towards the source of the microwave radiation will 'see' in their rest frame that radiation as having its frequency shifted, due to the first-order Doppler effect, by an amount $\omega_0 v'/c$ where $\omega_0 = 2\pi f_0$

† Since the ions are cooled by He gas introduced into the vacuum system, and both the gas and the vacuum system are close to room temperature, it follows that in this case the $^{199}Hg^+$ ions cannot be cooler than room temperature (~300 K).

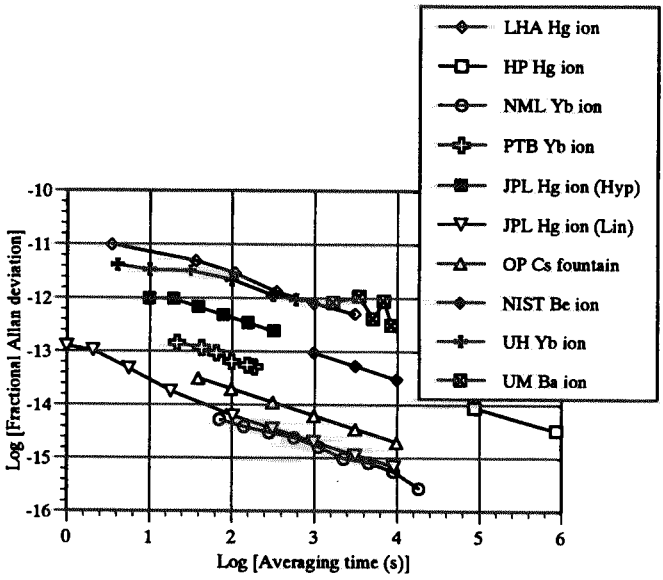

Figure 19. Demonstrated performance of the trapped-ion/trapped atom microwave frequency standards discussed in this review for which stability data have been published. Legend: LHA Hg ion: Laboratoire de l'Horloge Atomique (France) $^{199}Hg^{+}$, hyperbolic Paul ion trap (Jardino *et al* 1981a, b); HP Hg ion: Hewlett-Packard Laboratories (USA) $^{199}Hg^{+}$, hyperbolic Paul ion trap (Matsakis *et al* 1995); NML Yb ion: CSIRO National Measurement Laboratory (Australia) $^{171}Yb^{+}$, linear Paul ion trap (Fisk *et al* 1997); PTB Yb ion: Physikalisch-Technische Bundesanstalt (Germany) $^{171}Yb^{+}$, hyperbolic Paul ion trap (Schnier 1992, Tamm *et al* 1995); JPL Hg ion (Hyp): California Institute of Technology, Jet Propulsion Laboratory (USA) $^{199}Hg^{+}$, hyperbolic Paul ion trap (Prestage *et al* 1987a, b); JPL Hg ion (Lin): California Institute of Technology, Jet Propulsion Laboratory (USA) $^{199}Hg^{+}$, linear Paul ion trap (Tjoelker *et al* 1996a); OP Cs fountain: Observatoire de Paris (France) ^{133}Cs, atomic fountain (Clairon *et al* 1996a, b); NIST Be ion: National Institute of Standards and Technology (USA) $^{9}Be^{+}$, hyperbolic Penning ion trap (Bollinger *et al* 1991); UH Yb ion: University of Hamburg (Germany) $^{171}Yb^{+}$, hyperbolic Paul ion trap (Casdorff *et al* 1991); UM Ba ion: University of Mainz (Germany) $^{137}Ba^{+}$, hyperbolic Paul ion trap (Knab *et al* 1985).

is the angular frequency of the microwave radiation as measured in the laboratory rest frame. Integrating over all the thermal velocities present in the ensemble of ions leads to the conclusion that the effective bandwidth of the microwave radiation as seen by the ion cloud is given by equation (33). In contrast, a hypothetical single $^{199}Hg^{+}$ ion confined in the trap under discussion executes periodic sinusoidal motion at the secular frequency $\omega_s = 2\pi \times 50$ kHz, with a peak velocity component v' towards the source of the microwave radiation. The frequency of the microwave radiation as seen by the ion will be modulated by the first-order Doppler shift at the empty-trap secular frequency ω_s, and the effective magnetic vector $\boldsymbol{H}$ of the microwave field will be

$$\boldsymbol{H} = \boldsymbol{H}_0 \cos\left(\omega_0 t + \frac{\omega_0 v'}{\omega_s c} \sin \omega_s t\right). \tag{34}$$

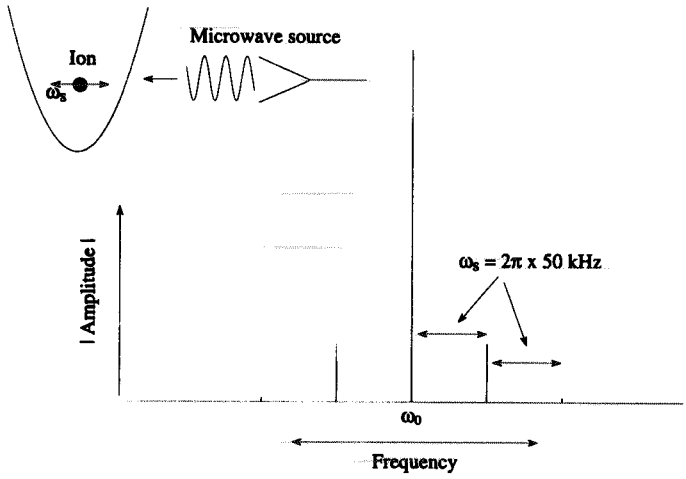

Figure 20. The amplitude spectrum of the microwave signal seen by a trapped $^{199}Hg^+$ ion at a temperature of 6000 K in a harmonic potential well characterized by a secular frequency $\omega_s = 2\pi \times 50$ kHz.

Equation (34) may be rewritten in a form which gives a better idea of its spectral composition;

$$\boldsymbol{H} = \boldsymbol{H}_0 \begin{bmatrix} J_0\left(\dfrac{\omega_0 v'}{\omega_s c}\right)\cos\omega_0 t \\ -J_1\left(\dfrac{\omega_0 v'}{\omega_s c}\right)(\cos(\omega_0-\omega_s)t - \cos(\omega_0+\omega_s)t) \\ +J_2\left(\dfrac{\omega_0 v'}{\omega_s c}\right)(\cos(\omega_0-2\omega_s)t + \cos(\omega_0+2\omega_s)t) \\ -J_3\left(\dfrac{\omega_0 v'}{\omega_s c}\right)(\cos(\omega_0-3\omega_s)t - \cos(\omega_0+3\omega_s)t) \\ +\cdots \end{bmatrix} \tag{35}$$

where $J_n(z)$ are Bessel functions of the first kind. Thus the ion sees the microwave spectrum as having discrete components spaced symmetrically about ω_0, and separated by the empty trap secular frequency ω_s (figure 20).

The central peak of the spectrum at ω_0 is unshifted and none of the peaks are broadened by the secular motion. The response of the ion to the microwave field will therefore be the same as it would be if the ion were stationary, provided the ion interacts only with the central peak. This condition will be met if the first-order Doppler shift due to the ion's motion is less than the secular frequency;

$$\frac{\omega_o v'}{c} < \omega_s \tag{36}$$

which may be simplified to

$$d < \frac{\lambda_0}{\pi} \tag{37}$$

where d is the amplitude of the secular motion and λ_0 is the wavelength of the microwave radiation. Dicke (1953) treats the case of a square potential well, yielding the similar result

$$d < \frac{\lambda_0}{2}. \tag{38}$$

The limitation on the spatial extent of the ions' motion expressed in equations (37) and (38) is often known as the Lamb–Dicke criterion, and indicates that if the motion of an ion, or a cloud of ions, in the direction of propagation of the interrogating radiation can be confined to a region of dimension less than half the wavelength of that radiation, then broadening due to the first-order Doppler effect will be absent. The Lamb–Dicke effect is one of the primary reasons trapped atoms and trapped ions are of interest as microwave frequency standards, since in the case of $^{199}Hg^{+}$ the ion must be confined within a 4 mm region to satisfy equation (37), which is readily achievable, allowing the clock transition to be resolved with precision limited in principle only by the duration of the microwave interrogation (equation (8)). If the Lamb–Dicke condition were not satisfied, the $^{199}Hg^{+}$ ion would need to be cooled to less than 10 μK to achieve the 3.5 Hz FWHM of the profile shown in figure 17.

4. Frequency offsets affecting trapped-ion standards

It is generally impractical to prepare and store a single ion, or ensemble of ions or atoms, without perturbing the frequency of the clock transition to a significant and observable extent. Ideally, the output frequency of an atomic frequency standard should reflect the *true clock frequency* of the atomic reference; that is, the frequency corresponding to the peak of the clock transition absorption resonance of a totally unperturbed, isolated atom or ion in a field-free vacuum. If this is achieved, the output of a frequency standard of any design, but using the same reference atomic species, will be the same.

It is therefore of interest to evaluate the perturbations to the clock frequency resulting from the configuration of a particular frequency standard. The uncertainty in the calculated frequency offset is then the uncertainty in the true clock frequency, and is generally referred to as the *accuracy* of the frequency standard.

The distinction between a frequency offset, a frequency drift and frequency noise is not clear, since a frequency perturbation is commonly referred to as noise if it fluctuates over a short period, as a drift if it fluctuates over longer periods and as an offset it does not change measurably during a given period of observation. The only clear distinction which can be made is between time-dependent frequency perturbations which can be expected on fundamental grounds to average to zero over some time scale, for example, shot noise, (see section 2.2) and those which do not. Because its effects average to zero in a properly designed frequency standard, shot noise generally affects only the stability of the frequency standard.

However, even if stability rather than absolute accuracy is important to the application of a particular frequency standard, the long-term stability of the standard will still generally be limited by the extent to which its frequency offsets are understood and can be controlled.

It is worth mentioning here that a further complication arises when one considers the precise meaning of the word *accuracy* in the context of a frequency standard. In section 2 we saw that the uncertainty in the measured frequency of a frequency standard generally varies with the time over which the measurement is averaged. However, when the accuracy of a frequency standard is quoted, an averaging time is seldom, if ever, given; the quoted value is usually the appropriately summed uncertainties in the measured or calculated frequency offsets of the standard. Recommendations on a consistent way of expressing the uncertainties in atomic frequency standards are presently under discussion (Fisk 1996).

In this section we consider the known causes of frequency offsets which do not average to zero over any time scale and which affect both the stability and the accuracy of trapped-ion frequency standards. In section 10.1 it will be seen that trapped-atom frequency standards

potentially have the advantage of being affected only by a subset of these phenomena, which of course is a primary motivation for their development. The magnitudes and sources of the frequency shifts, as far as they have been reported, affecting the trapped-atom/ion frequency standards discussed in this review are shown in table 2. The physics of these offsets is discussed in the following sections.

4.1. The quadratic Zeeman effect

All the common microwave atomic frequency standards require the atoms to be maintained in a finite and preferably uniform magnetic field (sometimes known for historical reasons as the 'C' field) in order to carry out high-resolution spectroscopy of the clock transition. This magnetic field lifts the degeneracy of the magnetic, or Zeeman, sublevels involved in the clock transition to the extent that the number of transitions between them is ideally negligible during the period Δt_R of the interrogation process. In the context of trapped-ion standards, transitions between the Zeeman sublevels of the clock transition may be induced by mechanical perturbations such as ion–ion collisions or collisions with buffer-gas atoms, and by electromagnetic radiation seen by the ions resulting from their secular motion in an inhomogeneous magnetic field. Consequently, the magnitude of the magnetic field required for a given frequency standard depends on several factors, and is probably determined empirically in most cases. A common symptom of transitions between the magnetic sublevels occurring during the interrogation period is poor visibility of the Ramsey fringes, due to the resulting loss of phase coherence between the reference atoms or ions and the interrogating microwave radiation. This is obviously undesirable, since it decreases the SNR of the error signal derivable from the Ramsey pattern.

The energy $E(F, M_F)$ of a particular Zeeman sublevel M_F of a hyperfine level F in a magnetic field B_0 is given by the Breit–Rabi equation† (Vanier and Audoin 1989, p 29)

$$E(F, M_F) = -\frac{E_{HFS}}{2(2I+1)} - g_I \mu_B B_0 M_F \pm \frac{E_{HFS}}{2}\left(1 + \frac{4M_F}{2I+1}x + x^2\right)^{\frac{1}{2}} \tag{39}$$

where

$$x = \frac{(g_I + g_J)\mu_B B_0}{E_{HFS}}. \tag{40}$$

In equations (39) and (40), E_{HFS} is the hyperfine splitting in energy units, g_J and g_I are the orbital and nuclear Landé g factors, I is the nuclear spin quantum number, μ_B is the Bohr magneton and the plus sign applies to the case where $F = I + J$ and the minus sign applies when $F = I - J$.

The effect of a magnetic field on the 40.5 GHz $F = 0 \rightarrow F = 1$ hyperfine transition in $^{199}Hg^+$ calculated according to equation (39) is shown in figure 21. As can be seen from equation (39), the energies of the $M_F = 0$ levels exhibit only a second-order dependence (*second-order Zeeman* effect or *quadratic Zeeman effect*) on the applied magnetic field, and consequently $M_F = 0 \rightarrow M_F = 0$ transitions are generally used as clock transitions in atomic frequency standards to minimize their sensitivity to magnetic-field fluctuations. In practice, magnetic fields of the order of a few tens of μT or less are used in the trapped-atom and trapped-ion standards discussed in this review, allowing simplification

† For magnetic fields stronger than about 1 mT, which are not used in most of the frequency standards discussed in this review, a recently identified additional term due to mixing of higher-energy electronic states into the ground state may become significant (Fortson 1987).

Table 2. Reported sources and fractional magnitudes of the larger frequency shifts affecting the trapped atom and trapped ion standards discussed in this review.

System	System type	Number of ions/atoms	Ion/atom temperature (K)	Quadratic Zeeman	Second order Doppler	Quadratic Stark	He buffer gas pressure (Pa)	Buffer gas shift
LHA Hg ion	Hyperbolic Paul $^{199}Hg^+$ 40.5 GHz	N/S	N/S	N/S	N/S	-3×10^{-14} [1]	None	0
HP Hg ion	Hyperbolic Paul $^{199}Hg^+$ 40.5 GHz	2×10^6 [2]	6000 [2]	$\sim 1 \times 10^{-14}$ [3]	-5×10^{-12} [3]	N/S	2×10^{-4} [3]	N/S
UM Ba ion	Hyperbolic Paul $^{137}Ba^+$ 8.04 GHz	10^5 [4]	N/S	N/S	-2×10^{-13} [4]	N/S	10^{-4} [4]	N/S
UH Yb ion	Hyperbolic Paul $^{171}Yb^+$ 12.6 GHz	N/S	N/S	N/S	N/S	N/S	None [5]	0
NIST Be ion	Penning $^{9}Be^+$ 303 MHz	5–10 $\times 10^3$ [a] [6]	< 0.25[b][6]	-1.3×10^{-14} [7]	-1.2×10^{-14} [7]	$< 1 \times 10^{-15}$ [7]	None [6]	0
JPL Hg ion (Hyp)	Hyperbolic Paul $^{199}Hg^+$ 40.5 GHz	N/S	~300 [8]	1.6×10^{-9} [8]	N/S	N/S	10^{-4} [8]	N/S
JPL Hg ion (Lin)	Linear Paul $^{199}Hg^+$ 40.5 GHz	2.5×10^6 [9]	~650	3×10^{-12} [9]	-8.8×10^{-13} [9]	N/S	10^{-3} [9]	1.1×10^{-13} [9]
PTB Yb ion	Hyperbolic Paul $^{171}Yb^+$ 12.6 GHz	N/S	2500 [10]	2×10^{-13} [10]	-2×10^{-12} [10]	-2×10^{-12}	10^{-3} [10]	5×10^{-13} [10]
NML Yb ion	Linear Paul $^{171}Yb^+$ 12.6 GHz	4×10^5 [11]	390 [11]	6×10^{-11} [11]	-7.4×10^{-13} [11]	-1×10^{-4} [11]	1.2×10^{-14} [11]	3×10^{-14} [11]
OP Cs fountain	Cs atomic fountain ^{133}Cs 9.19 GHz	$\sim 10^8$	$< 10^{-5}$ [b] [12]	1.5×10^{-13} [12]	$< 10^{-17}$ [12]	0	None [12]	0

[a] The quadratic Zeeman shift is not given by equation (40) in this case because the clock transition is not between two hyperfine levels—see references [6] and [7].

[b] The atoms/ions are laser-cooled.

N/S = not stated.

[1] Jardino *et al* (1981a, b), [2] Cutler *et al* (1987), [3] Matsakis *et al* (1995), [4] Knab *et al* (1985), [5] Casdorrf *et al* (1991), [6] Bollinger *et al* (1991), [7] Bollinger *et al* (1985), [8] Prestage *et al* (1987a), [9] Tjoelker *et al* (1993), [10] Schnier (1992), [11] Fisk *et al* (1997), [12] Clairon *et al* (1995).

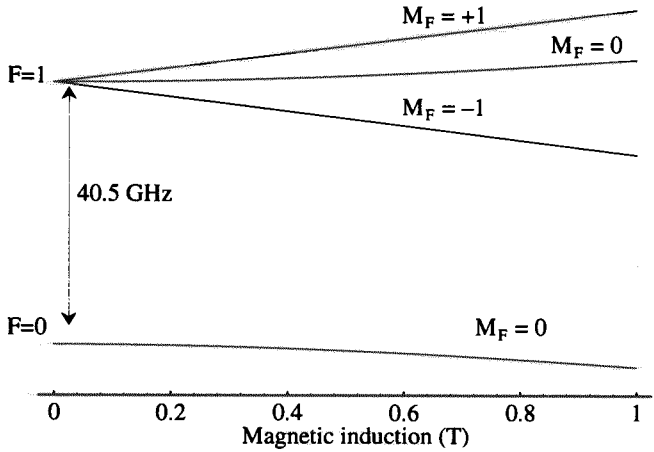

Figure 21. Zeeman splitting of the $^{199}Hg^{+}$ hyperfine transition.

of equation (39) to obtain the magnetic-field dependence of the frequencies f_0 and $f_{\pm 1}$ of the $M_F = 0 \rightarrow M_F = 0$ and $M_F = 0 \rightarrow M_F = \pm 1$ transitions respectively:

$$f_0 \approx f_{\mathrm{HFS}} + k_0 \langle B_0^2 \rangle \tag{41}$$

$$f_{\pm 1} \approx f_{\mathrm{HFS}} \pm k_{\pm} \langle B_0 \rangle. \tag{42}$$

The constants k_0 and $k_{\pm}$ for a number of ion species of interest for frequency standards purposes are tabulated in Vanier and Audoin (1989, p 37), and the angular brackets denote averaging over the spatial extent of the ion cloud;

$$\langle B_0 \rangle = \frac{\iiint n(\boldsymbol{r}) B_0(\boldsymbol{r}) \, \mathrm{d}^3 \boldsymbol{r}}{\iiint n(\boldsymbol{r}) \, \mathrm{d}^3 \boldsymbol{r}} \tag{43}$$

$$\langle B_0^2 \rangle = \frac{\iiint n(\boldsymbol{r}) B_0^2(\boldsymbol{r}) \, \mathrm{d}^3 \boldsymbol{r}}{\iiint n(\boldsymbol{r}) \, \mathrm{d}^3 \boldsymbol{r}}. \tag{44}$$

In the above equations, $n(\boldsymbol{r})$ is the spatial number-density distribution of the ions in the cloud.

Equation (41) is generally satisfactory down to accuracy levels in f_0 of about 10^{-14}; beyond this accuracy level the inclusion of higher-order terms in the series expansion of the square root in equation (39) must be considered.

The value of B_0 experienced by the atoms or ions in an atomic frequency standard is often determined by measuring the frequency difference, or Larmor frequency, between the $M_F = 0 \rightarrow M_F = 0$ and $M_F = 0 \rightarrow M_F = \pm 1$ transitions (figure 22), and then using the Breit–Rabi equation. The same equation may then be used to calculate the frequency offset of the $M_F = 0 \rightarrow M_F = 0$ clock transition due to the applied magnetic field.

In systems where the magnetic field is significantly inhomogeneous over the spatial extent of the ion cloud, for example in linear traps where the length of the ion cloud can be several centimetres, it is generally true that $\langle B_0 \rangle^2$ as measured from the Larmor frequency is not equal to $\langle B_0^2 \rangle$. In this case $B_0(\boldsymbol{r})$ must somehow be measured (Clairon *et al* 1995, Fisk *et al* 1996b, 1997), $n(\boldsymbol{r})$ must be determined using a model of the ion cloud (see next section), so that $\langle B_0^2(\boldsymbol{r}) \rangle$ may be calculated using equation (44) and finally the frequency offset $f_0 - f_{\mathrm{HFS}}$ due to the second-order Zeeman effect may be calculated using equation (41).

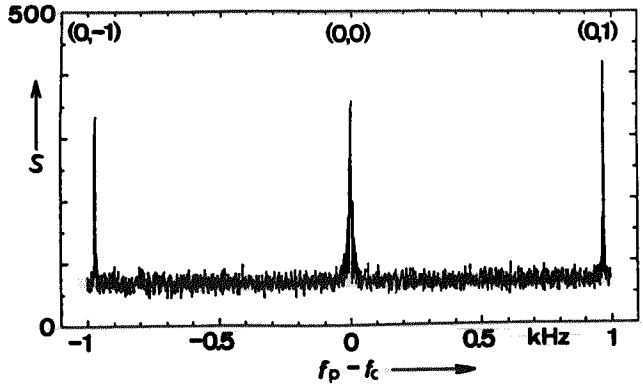

Figure 22. The ground-state hyperfine resonance spectrum of $^{171}Yb^+$ ions confined in a hyperbolic Paul trap. The three Zeeman components of the 12.6 GHz transition are visible, and their separation corresponds to a magnetic field of 0.07 μT. From Tamm *et al* (1995).

4.2. The second-order Doppler effect

The frequency f' 'seen' by an atom or ion moving with velocity v with respect to the laboratory rest-frame from where it is illuminated with radiation of frequency f is given by special relativity as

$$f' = f\sqrt{\frac{1-\frac{v}{c}}{1+\frac{v}{c}}}. \tag{45}$$

Expanding the square root as a power series, we obtain the frequency shift (the Doppler shift) $\Delta f_D = f - f'$:

$$\frac{\Delta f_D}{f} = \frac{v}{c} - \frac{1}{2}\left(\frac{v}{c}\right)^2 + \frac{1}{2}\left(\frac{v}{c}\right)^3 - \cdots. \tag{46}$$

The first term on the right-hand side of equation (46) is the first-order Doppler effect, and is eliminated for the purposes of most microwave trapped-ion and trapped-atom frequency standards by the previously discussed Lamb–Dicke effect. However, due to the stability of modern microwave frequency standards, frequency shifts due to the second term, known as the second-order Doppler shift or time-dilation shift, given by

$$\frac{\Delta f_{2OD}}{f} = -\frac{1}{2}\left(\frac{v}{c}\right)^2 \tag{47}$$

are significant and readily observable on atoms moving at thermal velocities.

Frequency shifts of atomic resonances due to the second-order Doppler effect are always in the direction of lower frequencies, and arise in trapped-ion frequency standards from a combination of the thermal secular motion and the RF micromotion of the trapped ions. The calculation of the resulting frequency shifts ideally requires a complete analytic model of the dynamics of the trapped ions. Such a model is not available, due to two principal difficulties (Schubert *et al* 1990): (i) the trapping potential is explicitly time-dependent, and (ii) the space charge of the ions couples the various spatial degrees of freedom. Consequently, calculation of the second-order Doppler shift relies on models of the ion clouds which are applicable in certain parameter regimes. In this section we shall summarize those models which have been most frequently used.

In the pseudopotential approximation, where it is possible notionally to separate the thermal secular motion of the ions from their RF micromotion, the RMS velocity $v_{\text{secular RMS}}$ associated with the secular motion of the ions in a confined cloud in thermal equilibrium characterized by a temperature T is given simply by

$$\langle v_{\text{secular RMS}} \rangle = \sqrt{\frac{3kT}{m}} \tag{48}$$

where k is Boltzmann's constant and m is the mass of the ion. The angular brackets denote time-averaging over one cycle of the motion.

The calculation of the velocity associated with the micromotion is more complicated, because the amplitude of the trapping RF field, and thus the velocity $v_{\text{micro RMS}}$ associated with the micromotion, increases from zero as we move away from the centre nodal point of a Paul trap. Consequently, as the number of ions in a trap increases, their mutual repulsion results in the cloud extending further into the region where the trapping RF amplitude is larger, thereby linking the component of the second-order Doppler shift due to the micromotion of the ions to the spatial distribution of the ions in the trapped cloud. The total second-order Doppler shift $\Delta f_{2\text{OD}}$ is then given by (Prestage *et al* 1990c)

$$\frac{\Delta f_{2\text{OD}}}{f} = -\frac{1}{2c^2}(\langle v_{\text{secular}}^2 + v_{\text{micro}}^2 \rangle) \tag{49}$$

where the averaging denoted by the angular brackets is again taken over one cycle of the secular motion, and also over the spatial extent of the ion cloud. For an ion cloud of sufficiently low density that the mutual interaction of the ions can be neglected, conservation of energy requires that, in the pseudopotential regime, the two terms inside the bracket of equation (49) must be equal, so that

$$\frac{\Delta f_{2\text{OD}}}{f} = -\frac{3kT}{mc^2}. \tag{50}$$

However, signal-to-noise considerations dictate that the low-density regime is not attractive for the purposes of a microwave frequency standard, and the mutual Coulomb repulsion of the ions must therefore be included in the calculation. More generally, when thermodynamic equilibrium exists, the second-order Doppler shift is given by

$$\begin{aligned} \left.\frac{\Delta f_{2\text{OD}}}{f}\right|_{\text{micro}} &= -\frac{1}{2Nc^2}\iiint n(\boldsymbol{r}) v_{\text{micro}}^2(\boldsymbol{r})\, \mathrm{d}^3\boldsymbol{r} \\ \left.\frac{\Delta f_{2\text{OD}}}{f}\right|_{\text{secular}} &= -\frac{3kT}{2mc^2} \end{aligned} \tag{51}$$

where N is the number of ions in the ion cloud and the integral is taken over the spatial extent of the cloud.

Jardino *et al* (1984) and, independently, Cutler *et al* (1985) have calculated the spatial density distribution of a cloud of ions in a spherical harmonic pseudopotential for a number of cloud temperatures (figure 23). At low temperatures the density profile is uniform across the cloud, with sharp edges. The reason for this becomes obvious when one notes that the total effective radial potential $\Phi_{\text{tot}}(r)$ seen by an ion is made up of the confining harmonic pseudopotential $\Psi(r)$ given by equation (30) and the space charge potential $\Phi_{\text{ion}}(r)$;

$$\Phi_{\text{tot}}(r) = \Psi(r) + q\Phi_{\text{ion}}(r) \tag{52}$$

where q is the charge on each ion. If the temperature of the ion cloud is sufficiently low, the mutual separation of the ions is determined purely by the combination of the confining force due to the pseudopotential and a repulsive force due to the charge of the ions. For such

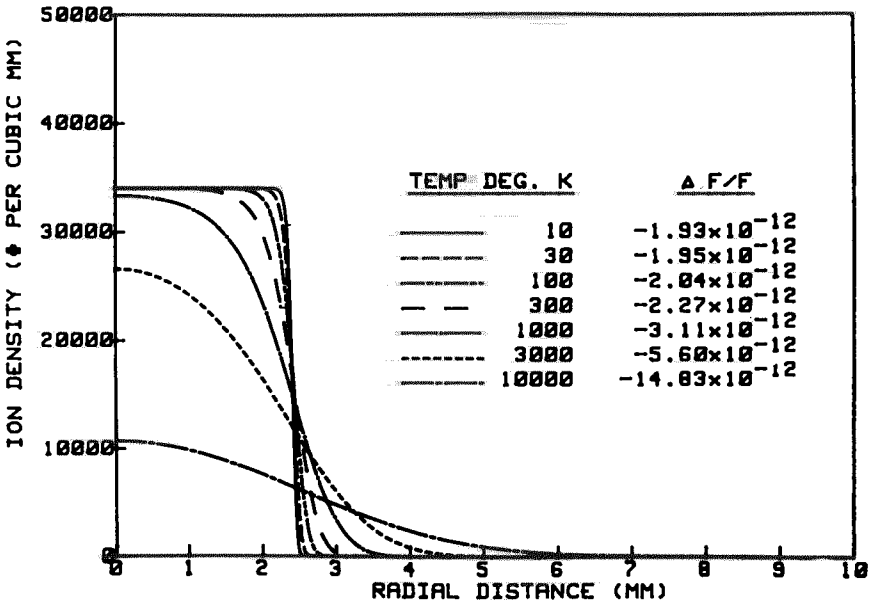

Figure 23. Calculated number-density distributions for 2×10^6 $^{199}Hg^+$ ions in a spherical harmonic pseudopotential for a number of cloud temperatures T. From Cutler *et al* (1985).

a cloud in equilibrium, $\Phi_{tot}(r)$ must be independent of r which, in view of equation (52), implies that $\phi_{ion}(r)$ must depend quadratically on r. Because the radial density profile $n(r)$ and $\Phi_{ion}(r)$ are related by the Poisson equation

$$\nabla^2 \Phi_{ion}(r) = -q\frac{n(r)}{\varepsilon} \tag{53}$$

$n(r)$ must therefore be independent of r out to the boundary of the ion cloud. As the temperature of the ion cloud increases, the thermal energy of the ions permits their excursion further out into the pseudopotential, and the edges of the ion cloud become less well defined.

In this 'cold-cloud' case, the uniform nature of $n(r)$ lends itself to a relatively simple expression for the second-order Doppler shift in a spherical pseudopotential characterized by a secular frequency ω confining n ions of mass m and charge q (Prestage *et al* 1990c):

$$\frac{\Delta f_{2OD}}{f} = -\frac{3}{10c^2}\left(\frac{n\omega q^2}{4\pi\varepsilon_0 m}\right)^{\frac{2}{3}}. \tag{54}$$

This expression is expected to be valid so long as the temperature is low enough so that the characteristic length (the Debye length) over which the ion-cloud density falls towards zero (figure 23) is small compared with the radius of the ion cloud. Inspection of figure 23 shows that this requirement is satisfied for the conditions corresponding to the calculations for temperatures less than approximately 500 K.

Prestage has also given an expression corresponding to equation (54) for the case of a linear Paul trap confining a cloud of ions of length L (Prestage *et al* 1990c):

$$\frac{\Delta f_{2OD}}{f} = -\frac{q^2}{8\pi\varepsilon_0 m c^2}\frac{n}{L}. \tag{55}$$

The expected fractional second-order Doppler shifts for a hyperbolic trap and a linear trap both containing 2×10^6 $^{199}Hg^+$ ions calculated using equations (54) and (55), assuming a

cloud length $L = 2$ cm in the linear trap and a typical secular frequency $\omega = 2\pi \times 50$ kHz for the hyperbolic trap, are 1.9×10^{-12} and 3.8×10^{-13} respectively. This five-fold reduction in the second-order Doppler shift in the linear trap for the same number of ions, and consequently the same SNR, is the primary motivation for the use of a linear Paul trap for frequency standards purposes. The physical reason for the reduced second-order Doppler shift in the linear trap for a given number of trapped ions is that the node of the trapping RF field is a line, rather than a point as is the case with a hyperbolic trap.

While Prestage's 'cold-cloud' model yields attractively simple expressions for the second-order Doppler shift, they are not always the most appropriate, first because the cold-cloud requirement may not be satisfied in many systems, and secondly because it is not always easy to measure the number N of ions in the trap with sufficient accuracy (see, for example, Gaboriaud *et al* 1981). Meis *et al* (1988) have given an alternative expression for the second-order Doppler shift in a hyperbolic trap in the 'hot-cloud' regime, where, due to their thermal energy, the density of ions in the trap is sufficiently low that the total radial potential $\Phi_{\text{ion}}(r)$ remains approximately harmonic in the presence of the space-charge of the ion cloud at temperature T

$$\frac{\Delta f_{2\text{OD}}}{f} = -\frac{kT}{mc^2}\left(\frac{3}{2} + \left(\frac{\omega_s}{\omega_m}\right)^2\right) \tag{56}$$

where T is given by

$$T = \frac{m\omega_m^2}{2\pi k}\left(\frac{0.23nq^2}{(\omega_s^2 - \omega_m^2)m\varepsilon_0}\right)^{\frac{2}{3}}. \tag{57}$$

Equation (56) has also been shown to be valid for a linear trap (Sellars *et al* 1995, Fisk *et al* 1997). In equations (56) and (57), ω_s is the secular frequency characterizing the motion of the ions when the trap is nearly empty, that is, in a ponderomotive pseudopotential which is not significantly distorted by the space charge of the ion cloud, and ω_m is the secular frequency corresponding to the trap being loaded to its normal operating level (see figure 24). If the number N of ions in the cloud is not known with sufficient accuracy, the temperature T may be measured spectroscopically (Prestage *et al* 1993a, Fisk *et al* 1994, 1997).

Cutler *et al* (1986) have addressed the problem of measuring the secular motion temperature T in the intermediate case between the hot- and cold-cloud regimes, where the space charge of the ion cloud results in a potential which is significantly anharmonic, but not a square well as in the cold-cloud case. They calculated the shape of the secular sidebands observed in a hyperbolic Paul trap by measuring the microwave frequency spectrum seen by the ions as they execute their secular trajectories (see also Enders *et al* 1992). The trajectories of the ions in this 'warm-cloud' regime are more complicated because, in the anharmonic potential, the ions do not execute simple harmonic motion, so that the trajectories must be calculated numerically from a set of initial positions and velocities of the ions. By fitting the calculated secular sideband spectrum to the observed spectrum from an ion cloud where the mass m, number of ions N and empty-trap secular frequency ω_s are known, the temperature T of the ion cloud is obtained. The density profile $n(r)$ is calculated by assuming thermodynamic equilibrium, allowing it to be written as

$$n(r) = C\exp\left[-\frac{\Phi_{\text{tot}}(r)}{kT}\right] \tag{58}$$

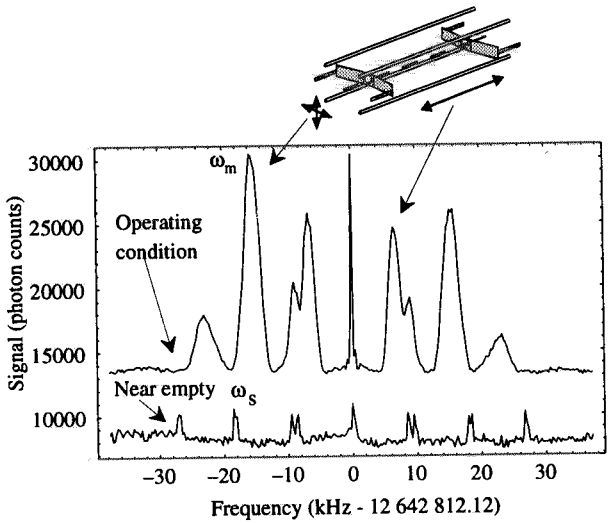

Figure 24. Sidebands on the microwave excitation spectrum of $^{171}Yb^+$ ions confined in a linear Paul trap. The sidebands occur due to the phase modulation of the microwave radiation seen by the ions as they execute their secular trajectories. The frequency of the secular motion decreases as the density of ions in the trap increases, due to space-charge distortion of the confining pseudopotential. From Fisk *et al* (1997).

where C is a constant. The requirement that $\Phi_{ion}(r)$ satisfies the Poisson equation (equation (53)) leads to a nonlinear second-order differential equation for $n(r)$:

$$n''(r) - \frac{n'(r)^2}{n(r)} + 2\frac{n'(r)}{r} - \frac{n(r)^2 q^2}{\varepsilon_0 kT} + \frac{3m\omega_s^2 n(r)}{kT} = 0. \tag{59}$$

Solving equation (59) for $n(r)$ (some solutions are shown in figure 23) and noting that the mean square velocity of the micromotion can be written

$$\langle v_{micro}^2(r)\rangle = \frac{\omega_s^2}{2} r^2 \tag{60}$$

allows the second-order Doppler shift to be calculated using equation (51). This method has been extended to the case of a linear Paul trap by Prestage *et al* (1993b).

4.3. The quadratic Stark effect

The electric fields associated with the ponderomotive trapping potential induce a frequency shift $\Delta f_{Q\text{Stark}}$ in the $M_F = 0 \rightarrow M_F = 0$ clock transition via the quadratic Stark effect. In $^2S_{1/2}$ states, this shift is towards lower frequencies:

$$\Delta f_{Q\text{Stark}} = -k_s \frac{\iiint n(\boldsymbol{r}) E_{Av}^2(\boldsymbol{r})\, d^3\boldsymbol{r}}{\iiint n(\boldsymbol{r})\, d^3\boldsymbol{r}}. \tag{61}$$

The quantity $E_{Av}^2(\boldsymbol{r})$ is the cycle-averaged square of the trapping electric field, and the coefficient k_s has been measured for $^{171}Yb^+$ as 2×10^{-21} m^2 V^{-2} (Tamm *et al* 1995) and has been calculated for $^{199}Hg^+$ as 3×10^{-22} m^2 V^{-2} (Jardino *et al* 1981a) and 1.43×10^{-22} m^2 V^{-2} (Itano *et al* 1982).

Under conditions where equation (56) is valid, and for a linear Paul trap, the quadratic Stark shift may be expressed analytically;

$$\Delta f_{Q\text{Stark}} = -4k_s \left(\frac{\omega_s}{\omega_m}\right)^2 \frac{m\Omega^2}{q^2} kT \tag{62}$$

where $\Omega/2\pi$ is the frequency of the RF trap drive (Fisk *et al* 1997).

A frequency shift, related to the Stark effect, due to the oscillating electric field of the background black-body radiation, affects all atomic frequency standards (Audoin 1997, Hollberg and Hall 1984, Itano *et al* 1982). For the ^{133}Cs clock transition the resulting calculated fractional frequency shift is

$$\Delta f_{Q\text{Stark}} = -1.69(4) \times 10^{-14} \left(\frac{T}{300}\right)^4 \tag{63}$$

where the background temperature T (typically room temperature) is expressed in Kelvin (Itano *et al* 1982). The corresponding shift in other atomic species will depend on their hyperfine polarizabilities. Because the black-body shift is not unique to trapped-atom or trapped-ion frequency standards, the reader is referred to the above references for further details.

4.4. The helium pressure shift

The helium introduced as a buffer gas into the vacuum systems of a number of trapped-ion frequency standards generally causes a shift in the clock frequency due to collisions between the trapped ions and the helium atoms. The helium also reduces the temperature of the ion cloud (the principal reason for its use), which results in a further frequency shift due to a reduction in the second-order Doppler shift. A typical example of the measured dependence of the frequency of a trapped-ion standard on the pressure of the helium buffer gas is shown in figure 25. As the helium pressure is increased from zero, the frequency of the standard increases rapidly, due to a lowering of the ion-cloud temperature (Lunney *et al* 1992), and a consequent reduction in the second-order Doppler shift. As the helium pressure increases further, the ion-cloud temperature stabilizes, and the frequency of the standard increases more slowly and linearly as the collision rate between the ions and the helium atoms increases linearly. Corresponding curves having similar shapes have been observed in other systems (e.g. Cutler *et al* 1985, Fisk *et al* 1995b).

The collisional shift due to the helium buffer gas is usually determined by extrapolating the linear region of the frequency versus the helium pressure curve to zero helium pressure.

Nitrogen and methane (Bauch *et al* 1996) have been shown to result in a frequency shift in the opposite direction to that of helium when introduced at sufficient partial pressure into a trapped $^{171}Yb^+$ ion standard (figure 26), raising the possibility that an appropriate mixture of helium and either of these other gases could result in a very small frequency dependence on buffer-gas pressure. However, in the case of $^{171}Yb^+$, nitrogen has also been shown to affect the population of metastable levels (Seidel and Maleki 1995a, b), and the consequences (some of which may be beneficial) of these effects on the operation of a frequency standard have not been fully investigated.

Frequency shifts attributed to the presence of other gases as impurities in the vacuum system have also been observed (Bollinger *et al* 1991), but are generally not understood in detail.

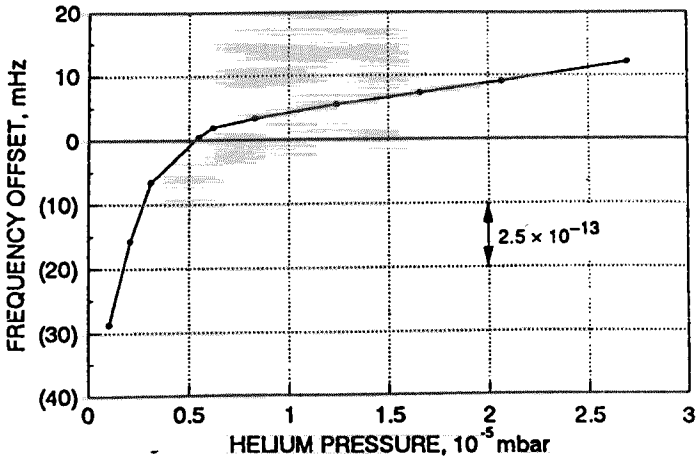

Figure 25. Measured frequency shift versus helium buffer-gas pressure in a cloud of $^{199}Hg^+$ ions confined in a linear Paul trap. From Tjoelker *et al* (1993).

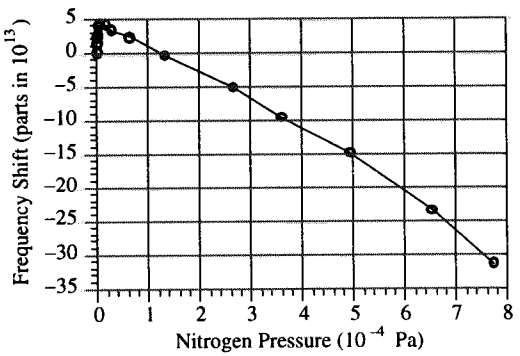

Figure 26. Dependence of the 12.6 GHz clock frequency of $^{171}Yb^+$ ions confined in a linear Paul trap on the pressure of nitrogen introduced into the vacuum. (Not published elsewhere.)

5. $^{199}Hg^+$ microwave frequency standards

Since the development of the pioneering $^{199}Hg^+$ microwave frequency standards discussed earlier in this review, much of the development work on $^{199}Hg^+$ standards has taken place at the NASA Jet Propulsion Laboratory (JPL). A 40.5 GHz frequency standard (referred to here as JPL Hg ion (Hyp)—see table 2 and figure 19), based on a cloud of $^{199}Hg^+$ ions confined in a hyperbolic trap, and operating in a similar manner to the HP and LHA standards discussed in section 3.3, was developed by Prestage, Maleki and Dick (Maleki 1981, Prestage *et al* 1987a, b). The stability performance of this system ($4.4 \times 10^{-12}\tau^{-1/2}$) is remarkably consistent with that of the HP $^{199}Hg^+$ standard (figure 19) (Matsakis *et al* 1995). In the late 1980s, Prestage *et al* (1988, 1989, 1990c) recognized advantages of the nodal region of the confining RF fields being a line in a linear trap, rather than a point in a hyperbolic trap. The JPL group was the first to demonstrate a microwave frequency standard based on ions confined in a linear trap.

The performance of the helium buffer-gas-cooled JPL linear ion-trap system (JPL $^{199}Hg^+$ (Lin) see table 2 and figure 19) has improved steadily over a period of several years as factors

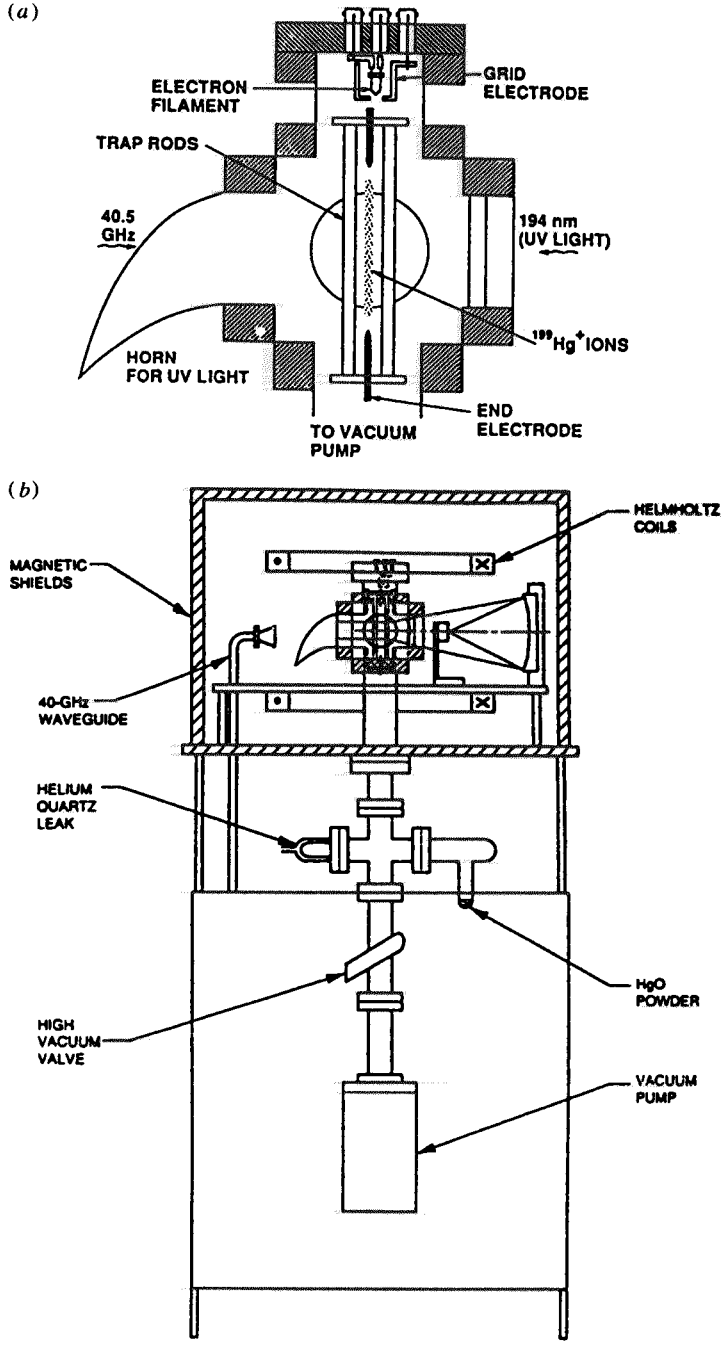

Figure 27. Schematic diagram of the JPL linear $^{199}Hg^{+}$ ion trap system. $^{199}Hg^{+}$ ions are generated by heating HgO to produce Hg vapour, and ionizing the Hg atoms using electrons emitted along the longitudinal axis of the trap. The Helmholtz coils provide control of the magnetic field within the trap, and the magnetic shielding isolates the ion cloud from magnetic fluctuations in the laboratory environment. The pressure of helium in the system is monitored with an ionization gauge, and controlled by adjusting the temperature of a quartz membrane through which the helium passes. From (*a*) Tjoelker *et al* (1993) and (*b*) Prestage *et al* (1993b).

such as magnetic shielding and passive stabilization of the number of ions in the trap have been improved (Prestage and Maleki 1994, Prestage *et al* 1990a, b, 1991, 1992a, b, 1993a, Tjoelker *et al* 1993, 1994, 1995, 1996a, b). The system has exhibited an extraordinary stability performance $\sigma_y(\tau) = 6.5 \times 10^{-14}\tau^{-1/2}$ for $\tau < 10^4$ s (figure 19), which has not yet been significantly surpassed by any passive frequency standard.

One disadvantage with the linear-trap configuration compared with the hyperbolic configuration is that it is more difficult to maintain a homogeneous magnetic field along the length (up to several cm) of the ion cloud. The variation in the magnetic field experienced by the ions as they execute their secular trajectories along the longitudinal axis of the trap tends to result in transitions between the Zeeman sublevels, resulting from (a) the Zeeman sublevels becoming degenerate at some point in the trajectory, and (b) coincidences between the secular frequencies (and their harmonics) and the Larmor frequency. As discussed in section 4.1, these transitions reduce the visibility of the Ramsey fringes.

The usual solution to this problem has been to apply significantly greater magnetic fields in linear trap systems, for example 40 mG in the case of the JPL $^{199}Hg^+$ (Lin) system (Tjoelker *et al* 1996a) and 8 μT in the case of the NML $^{171}Yb^+$ system (Fisk *et al* 1996a). In comparison, the PTB $^{171}Yb^+$ system, which uses the hyperbolic trap configuration, requires only 70 nT (Tamm *et al* 1995). Lower magnetic fields are desirable, since they reduce the sensitivity of the standard to magnetic fluctuations, which can be understood by differentiating equation (41):

$$\frac{\partial f_0}{\partial B_0} = 2k_0\langle B_0\rangle. \tag{64}$$

A new and innovative modification to the linear Paul trap configuration which is intended to overcome the above problems has been developed by Prestage *et al* (1993b, 1994, 1995). This new design (figure 28) allows the ions to be electrostatically moved into a narrow, highly shielded and magnetically homogeneous waveguide region of the trap for the microwave interrogation part of the measurement cycle, and then shifted into a second region for the optical part of the cycle.

The improved design is expected to yield a performance $\sigma_y(\tau) = 2 \times 10^{-14}\tau^{-1/2}$ (Tjoelker *et al* 1996a).

The unprecedented stability performance of the JPL $^{199}Hg^+$ standards is achieved in part by using a relatively large and consequently hot cloud of ions to obtain a good SNR for the microwave interrogation. This necessarily results in a significant second-order Doppler shift (table 2) due to the edges of the cloud extending (about one or two mm) away from the nodal region of the trapping RF field. The accuracy of the JPL standards, like other ion-trap standards using large ion clouds, is limited by the difficulty of accurately calculating the second-order Doppler shift without making approximations and idealizations which may not be fully justified.

An obvious solution to the above problem of accurately calculating the second-order Doppler shift is to reduce it to negligible proportions by:

- cooling the ion cloud to extremely low temperatures to reduce the secular motion;
- reducing the number of ions to one in a hyperbolic trap, or in the case of a linear trap, to a sufficiently small number so that they all lie along the nodal line of the confining RF field, and thus execute no micromotion.

Cooling of atoms (and ions) to temperatures well below 1 K can be achieved using a technique known as laser-cooling, where the momentum of optical photons tuned near to resonance is used to dissipate the momentum of the atoms by a series of absorption and spontaneous emission processes. A detailed discussion of laser-cooling of trapped ions is

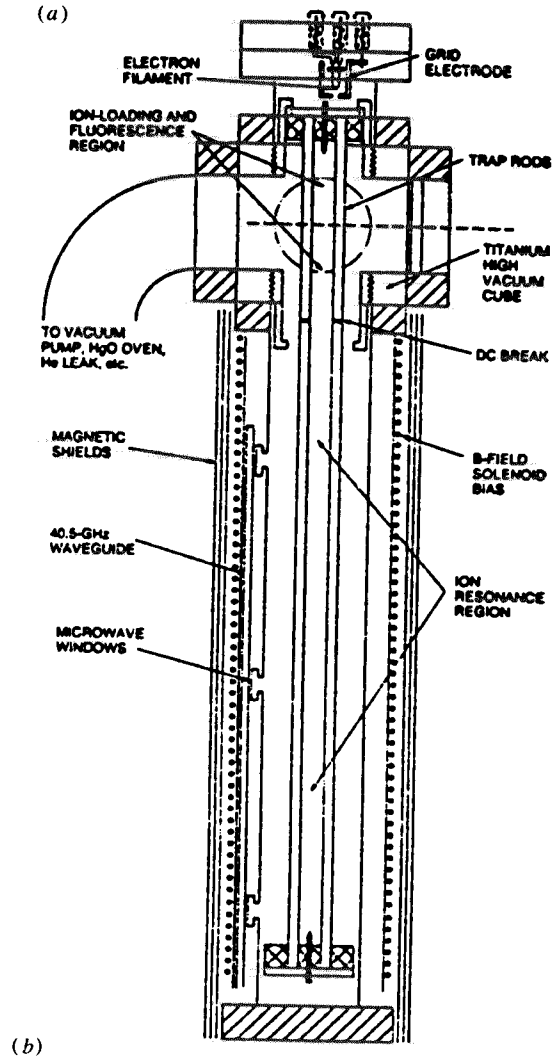

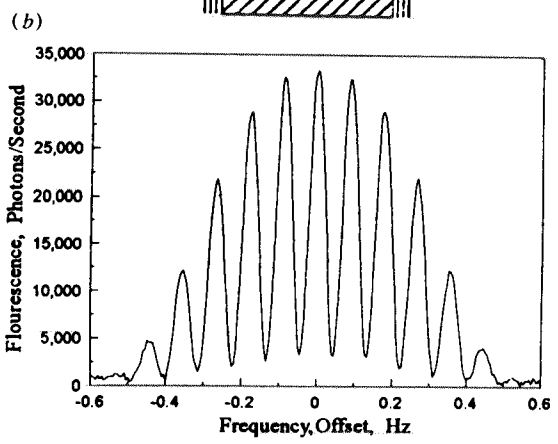

Figure 28. (*a*) The improved Prestage linear ion trap frequency standard. ^{199}Hg atoms are ionized and optically state-prepared in the upper region of the trap, then transferred electrostatically to the lower region where they are interrogated with 40.5 GHz microwave radiation. The ions are then moved back to the upper region to measure optically the fraction of the population which absorbed a microwave photon. Dimensions are 10 × 50 cm. From Prestage *et al* (1993b). (*b*) Ramsey fringes resulting from a $\Delta t_R = 11.1$ s interrogation cycle in the improved Prestage standard. From Tjoelker *et al* (1996a).

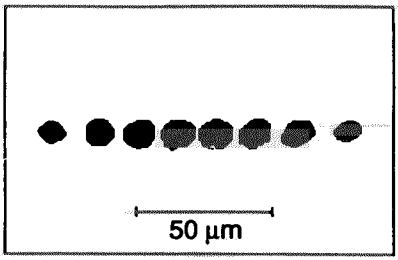

Figure 29. Image of a string of eight cold (<1 mK) $^{199}Hg^+$ ions arranged along the longitudinal axis of a linear Paul trap. The ability to image the ions individually means that each ion can be regarded as an independent atomic clock. From Raizen *et al* (1992).

beyond the scope of this review, but the subject has been well covered in a number of other reviews (see, for example Itano *et al* 1995, Wineland and Itano 1983, Blatt *et al* 1992), and also in the context of fundamental limits to frequency metrology (Wineland *et al* 1987, 1996, Wineland and Itano 1987, Wineland 1984).

The research group led by Wineland at the US National Institute of Standards and Technology (NIST) has made impressive conceptual and experimental progress towards RF, microwave and optical frequency standards based on extremely cold ions (Wineland 1981, Wineland *et al* 1981, 1989, 1990a, b, 1996, Bollinger *et al* 1985, 1989, 1991, Bergquist *et al* 1991, Raizen *et al* 1992, Poitzsch *et al* 1994, 1996, Miller *et al* 1995). In particular, a microwave frequency standard based on a 'string' consisting of a few tens of $^{199}Hg^+$ ions laser-cooled to temperatures less than 10^{-3} K arranged along the nodal line of a linear trap (figure 29) is in the advanced stages of development. Under such conditions, a reduction of the fractional second-order Doppler shift to around -2.3×10^{-18} (cf table 2) and an unprecedented total fractional accuracy of better than ± 1 part in 10^{-16} is thought possible (Wineland *et al* 1987, Miller *et al* 1995, 1996). In order to achieve such accuracies, background impurity gases which may cause collisional and chemical perturbations to the 40.5 GHz clock transition are, rather heroically, minimized by cooling the ion trap, its associated optics, microwave antenna, RF drive and vacuum enclosure to 4.2 K in a liquid-helium cryostat.

The SNR and thus the short-term stability performance of the NIST cryogenic trapped-ion standard will be limited by the relatively small number of ions interrogated by the microwave field (see figure 11 and equation (19)). Consequently, it is likely that this system will be operated periodically rather than continuously, and will serve as an extremely accurate frequency calibration for other less accurate frequency standards.

6. $^{137}Ba^+$ microwave frequency standards

Another early demonstration of a trapped-ion frequency standard (denoted UM $^{137}Ba^+$, performance shown in figure 19, see also table 2) used the 8.04 GHz ground-state hyperfine transition in $^{137}Ba^+$ ions confined in a hyperbolic Paul trap (figure 30) (Knab *et al* 1985).

About 10^5 $^{137}Ba^+$ ions were cooled by helium as a buffer gas in a hyperbolic trap with dimensions $r_0 = 20.0$ mm and $z_0 = 14.1$ mm (see figure 13). The ions could be stored for several hours. A pulsed dye laser tuned to the 493.4 nm optical transition served to optically pump the population into the $F = 1$ hyperfine level of the ground electronic state before microwave interrogation, and to detect population in the $F = 2$ level after interrogation. The measured stability performance of the UM $^{137}Ba^+$ standard (figure 19) was apparently

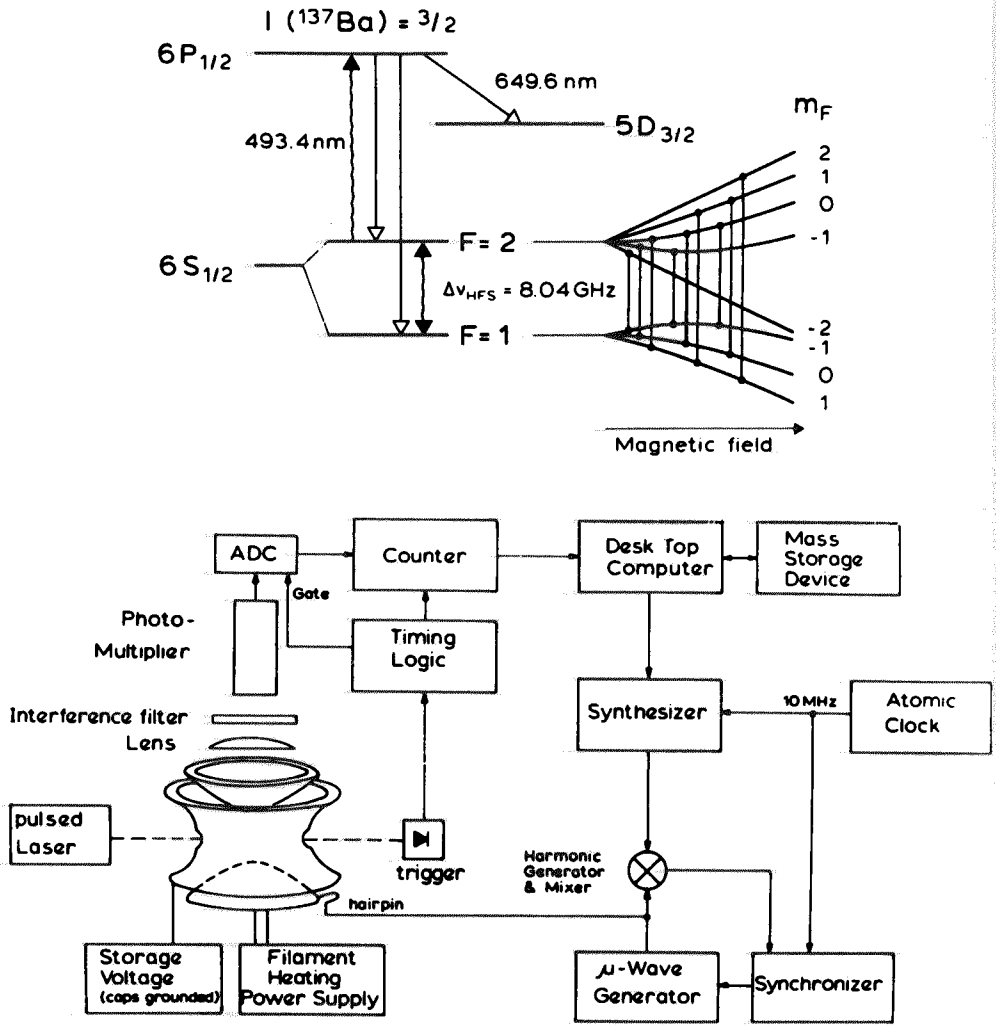

Figure 30. Level scheme and experimental arrangement of the UM $^{137}Ba^{+}$ prototype 8.04 GHz microwave frequency standard. From Knab *et al* (1985).

limited by the performance of the conventional Cs standard used as a frequency reference.

7. $^{9}Be^{+}$ microwave frequency standards

The first application of laser-cooled trapped ions as an atomic frequency standard was the NIST $^{9}Be^{+}$ system (figure 19) (Bollinger *et al* 1983, 1985, 1989, 1991, see also Imajo *et al* 1992). The $^{9}Be^{+}$ standard is different from the others described in this review in that the 303 MHz RF clock transition is between two Zeeman-split sublevels of the $F = 1$ ground-state hyperfine level (figure 31). This scheme was chosen because at the relatively large magnetic induction $B_0 = 0.8194$ T, the frequency of the clock transition is independent of the magnetic field to first order. A magnetic field of this magnitude is conveniently available in a Penning-type ion trap.

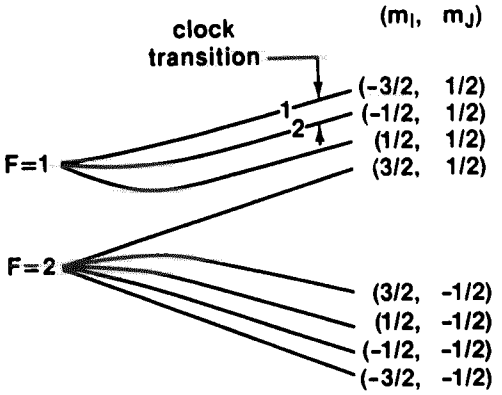

Figure 31. Hyperfine energy levels (not drawn to scale) of the $^9Be^+$ ground state, as a function of the magnetic field (horizontal axis). At a magnetic induction $B_0 = 0.8194$ T the 303 MHz clock transition is independent of magnetic field to first order. From Bollinger *et al* (1991).

Light at 313 nm, generated by frequency-doubling a dye laser, was used to prepare the $^9Be^+$ ions in the $(-\frac{3}{2}, -\frac{1}{2})$ state, and to detect ions which had absorbed 303 MHz photons at the end of the measurement cycle. The hyperbolic Penning trap was loaded with between 5000 and 10 000 $^9Be^+$ ions and between 50 000 and 100 000 $^{26}Mg^+$ ions. A second laser-derived light source at 280 nm was used to cool the $^{26}Mg^+$ ions, which *sympathetically* cooled the $^9Be^+$ ions to less than 0.1 K via their mutual Coulomb interaction. The reason for using the sympathetic cooling scheme was to avoid having cooling light resonant with the $^9Be^+$ ions illuminating the ion cloud during the RF interrogation cycle. This near-resonant light would otherwise introduce a shift (the *light shift* see, for example, Cohen-Tannoudji *et al* (1992)) in the energies of the levels involved in the clock transition.

The stability of the frequency standard was measured to be better than $\sigma_y(\tau) = 3 \times 10^{-12}\tau^{-1/2}$ for $\tau < 10^4$ s (figure 19), which is within a factor of 4 of the theoretical limiting value based on the number of ions used (see equation (21)). For $\tau > 10^6$ s the fractional stability of the standard was apparently limited to about $\sigma_y(\tau) = 3 \times 10^{-14}$ by a shift due to the presence of residual background gases in the vacuum system. The details of this shift are not yet understood. If the spurious pressure shift can be eliminated, the relatively small second-order Doppler shift ($(-1.2 \pm 0.5) \times 10^{-14}$), which results from the absence of micromotion of the ions in the Penning trap and the low temperature of the ions, may make an accuracy of better than $\pm 5 \times 10^{-15}$ achievable (Bollinger *et al* 1991, Tan *et al* 1995).

8. $^{171}Yb^+$ microwave frequency standards

The possible application of $^{171}Yb^+$ (figure 32) as a 12.6 GHz microwave frequency standard was first investigated by Blatt *et al* (1982).

The attraction of $^{171}Yb^+$ is that laser light at 369.5 nm can be generated by frequency-doubling relatively inexpensive, compact and reliable diode laser-based systems (see, for example, Tamm 1993, Tamm and Schnier 1992, Seidel *et al* 1992), rather than the complex and expensive laser systems used for the NIST $^{199}Hg^+$ and $^9Be^+$ standards. Consequently, the possible use of $^{171}Yb^+$ in a microwave frequency standard has probably received attention from a greater number of research groups than any other ion species.

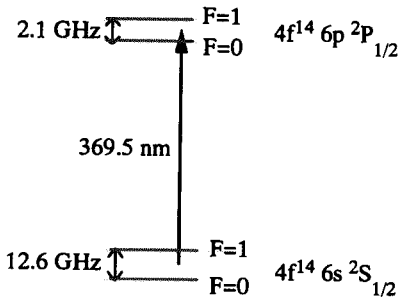

Figure 32. Partial energy-level diagram of $^{171}Yb^+$, showing the 12.6 GHz clock transition.

The group led by Blatt at the University of Hamburg achieved the first demonstration of a $^{171}Yb^+$ microwave frequency standard (designated UH Yb in figure 19 and table 2), which yielded a performance $\sigma_y(\tau) = 2 \times 10^{-11}\tau^{-1/2}$ for averaging times τ less than 1000 s. The system used the hyperbolic Paul trap configuration (Casdorff *et al* 1991, Blatt *et al* 1989). In subsequent years, prototype $^{171}Yb^+$ standards of progressively superior performance have been developed, or are under development, by other workers in both hyperbolic (Schnier 1992, Schnier *et al* 1992, Bauch *et al* 1996, Tamm *et al* 1995) and linear Paul trap configurations (Fisk *et al* 1994, 1995a, b, 1996a, b, 1997, Sellars *et al* 1995, Seidel and Maleki 1994).

The Blatt group has also pursued a microwave frequency standard based on a single $^{171}Yb^+$ ion, laser cooled in a hyperbolic Paul trap to less than 0.1 K. A microwave resonance of FWHM 40 Hz has been observed, corresponding to a microwave interrogation time (duration of the single microwave pulse) of about 20 ms (see figure 4) (Enders *et al* 1993). The microwave interrogation time is presently limited by the requirement that during this time the cooling 369 nm laser must be blocked in order to avoid light shifts in the microwave resonance frequency. When longer interrogation times are used, the ion temperature increases due to the prolonged absence of the cooling laser (Fisk *et al* 1993a, b, Dehmelt 1967, 1969, Cutler *et al* 1985, 1987, Blümel *et al* 1989). This problem is addressed in the NIST $^9Be^+$ system by using a second ion species to sympathetically cool the $^9Be^+$ ions, as described in section 7. A potential accuracy of better than ± 1 part in 10^{16} is predicted for the single cold $^{171}Yb^+$ ion standard (Enders *et al* 1993).

A phenomenon noticed by most who have studied trapped Yb^+ ions is that there is a tendency for the fluorescence signal from the ion cloud to deteriorate when illuminated with resonant 369 nm laser radiation. The deterioration of signal occurs despite the presence of resonant 12.6 GHz radiation in $^{171}Yb^+$; it has been observed in all naturally occurring isotopes of Yb and is not always associated with loss of ions from the trap. This phenomenon has been attributed to populations being 'trapped' in long-lived metastable states, with lifetimes of up to 8 days, via spontaneous emission from the $^2P_{1/2}$ level (Gerz *et al* 1988, Lehmitz *et al* 1989).

Loss of signal from the ion cloud is obviously inconvenient, and considerable effort has been devoted to understanding and overcoming this problem. It has been found that illumination of the ion cloud with light at various wavelengths can at least partially recover the lost signal, presumably by depopulating the metastable levels (Bauch *et al* 1992, Seidel *et al* 1992, Sugiyama and Yoda 1993, Gill *et al* 1995, Klein *et al* 1991, Fisk *et al* 1993a, Blatt *et al* 1989). There is also evidence that, in addition to loss of signal due to population of metastable states, the excited Yb^+ ions may react with background impurity gases in

Table 3. Reported frequencies of the $^{171}Yb^+$ 12.6 GHz clock transition, corrected to correspond to that of an ion in free space unperturbed by any external forces or fields.

Corrected $^{171}Yb^+$ clock frequency (Hz)	Reference
12 642 812 124.2 ± 1.4	Blatt *et al* 1982
12 642 812 118.471 ± 0.009	Bauch *et al* 1993
	Tamm *et al* 1995
12 642 812 118.468 ± 0.0016	Sellars *et al* 1995
12 642 812 118.466 ± 0.002	Fisk *et al* 1997

the vacuum system, to form molecules which may or may not remain in the trap but in any case will no longer exhibit resonance with the 369 nm interrogation light (Yoda and Sugiyama 1992a, b, Sugiyama and Yoda 1992, 1993, 1995, 1997). More work will be required before the mechanisms causing the loss of fluorescence signal from Yb^+ ions when they are illuminated with resonant 369 nm light are fully understood.

Significant attention has been paid to the accurate calculation of the frequency of the 12.6 GHz $^{171}Yb^+$ clock transition, after correction for the known perturbations (discussed in section 4) caused by the environment within the ion trap. The reported frequencies are given in table 3. The variation in the reported frequencies reflects the difficulty of identifying all perturbations and establishing the validity of the approximations which must be made in order to make the calculation of the frequency corrections tractable, and also the difficulty in realizing the SI second with the required accuracy in a particular laboratory (see, for example, Quinn 1991, Sullivan and Levine 1991). Nevertheless, if the more recent reported frequencies are correct, the $^{171}Yb^+$ 12.6 GHz clock frequency is one of the most accurately known physical constants.

9. $^{113}Cd^+$ microwave frequency standards

The ground-state hyperfine splitting of $^{113}Cd^+$ ions confined in a hyperbolic Paul trap has recently been measured as 15 199 862 858 ± 2 Hz, in a preliminary investigation of the suitability of this ion as a microwave frequency standard (Tanaka *et al* 1996). The microwave interrogation and optical detection scheme was similar to that used in the investigations of $^{171}Yb^+$, but with an optical wavelength of 214.5 nm. No frequency stability data has yet been reported.

10. Trapped-atom microwave frequency standards

Because the 9.1 GHz ground-state hyperfine splitting in the ^{133}Cs (figure 33) atom defines the second in SI units, a Cs-based microwave frequency standard of superior stability and accuracy to conventional Cs beam standards will be a device of great importance as a primary standard of frequency for many years to come. Like the motivation for developing trapped-ion standards, an attractive strategy for improving the Cs standard is to increase the interaction time between the microwave radiation and the atoms, and to reduce systematic shifts, such as the second-order Doppler shift. Both these aims can in principle be achieved by confining and laser cooling the atoms. Due to their lack of charge, ^{133}Cs atoms cannot be confined in the Paul traps discussed in the previous sections, and ionizing the atoms would not be a useful procedure since the magnetic moment of the electron cloud circulating around the nucleus would change, and consequently so would the ground state hyperfine splitting.

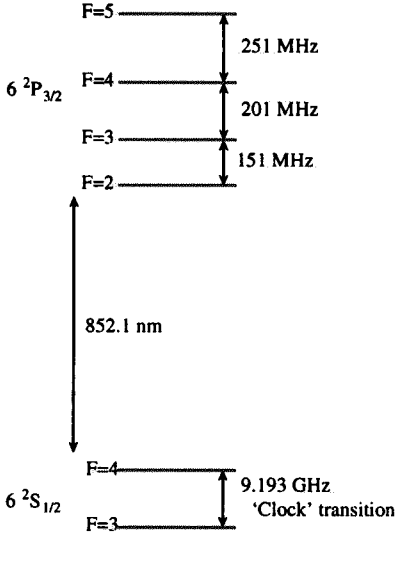

Figure 33. Partial energy-level diagram (not to scale) of the ^{133}Cs atom. Lasers tuned to particular hyperfine components of the 852.1 nm optical transition are used for optical cooling and trapping of the atoms, preparation of the atoms in the $F = 3$ component of the ground state prior to interrogation by the 9.193 GHz microwave radiation, and subsequent measurement of the fraction of atoms excited to the $F = 4$ component of the ground state by the microwave radiation (Clairon *et al* 1991).

However, cooling and trapping of Cs atoms in a device known as a magneto-optical trap (MOT) is now a well-established technique (Raab *et al* 1987, Monroe *et al* 1990, Phillips *et al* 1991, Gibble *et al* 1992); for reviews of laser cooling of atoms see, for example, Metcalf and Van der Straten (1994) and Foot (1991); for discussion of the application of laser cooling of atoms to frequency standards purposes see Gibble and Chu (1992) and Rolston and Phillips (1991). Another technique of atom cooling, known as optical molasses, where the atomic velocity is damped due to interaction of atoms with polarization gradients in optical standing waves generated by six orthogonal lasers, is capable of lower ultimate atom temperatures than the MOT, but is limited also to lower atom cloud densities (see, for example, Dalibard and Cohen-Tannoudji 1989).

10.1. The OP Cs fountain microwave frequency standard

Optical cooling and trapping of Cs atoms involves the use of saturating laser light tuned to near resonance with the hyperfine components of the 852.1 nm optical transition (Sesko and Wieman 1989). Unfortunately this laser light results in a light shift in the energies of the levels between which it is tuned, and this shift can be of the order of the Rabi frequency (several MHz or more) characterizing the interaction between the light and the atoms (for a discussion of the Rabi frequency see, for example, Shen (1984), Allen and Eberly (1975) and Cohen-Tannoudji *et al* (1992)). The relatively large frequency shift in the clock transition results in the environment within a MOT or optical molasses being quite unsuitable for the ^{133}Cs atoms used as a microwave frequency reference. The highly elegant solution to this problem, shown in figure 34, is commonly known as the Cs fountain (Hall *et al* 1989). The Cs fountain involves using the cooling lasers to launch a ball of very cold (a few μK) atoms, cooled in either a MOT or optical molasses or a sequential combination of the two, onto a ballistic trajectory upwards through a continuously energized microwave cavity, allowing them to fall back through the cavity, and detecting the fraction of atoms which were excited by the resulting Ramsey double-pulse of microwave radiation (Kasevich *et al* 1989, Clairon *et al* 1991, Gibble and Chu 1993, Ohshima *et al* 1995). An alternative scheme, whereby the Cs atoms are dropped from the MOT and interrogated with microwave radiation as they fall, has also been demonstrated (Monroe *et al* 1991). Because in both

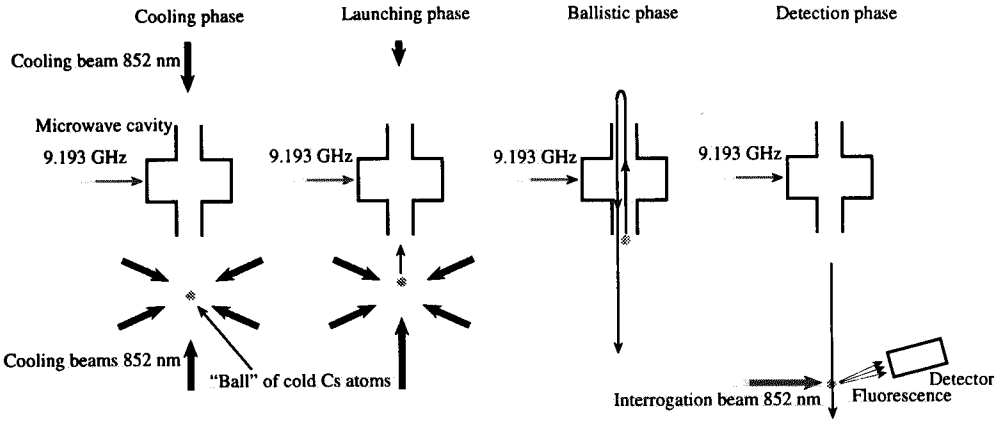

Figure 34. Schematic diagram of a Cs fountain. A 'ball' of Cs atoms a few mm in diameter is cooled from a room-temperature vapour to below 10 μK and confined by radiation pressure in either a MOT or optical molasses (or a sequential combination of the two) formed by six orthogonal 852.1 nm laser beams. The atoms are also prepared in the $F = 3$ hyperfine component of the ground state. After the cooling phase, the frequencies of the two laser beams counter-propagating in the vertical direction are adjusted to launch the ball of cold atoms onto a ballistic trajectory upwards through the microwave cavity, where they experience a microwave pulse at the clock frequency. After falling back down through the cavity, where they experience a second microwave pulse, the fraction of atoms which underwent the clock transition is measured using a seventh laser beam tuned to the $F = 4 \rightarrow F = 5$ hyperfine component of the 852.1 nm optical transition.

cases the interrogation of the atoms by the microwave radiation takes place when the atoms are in free-fall in a high vacuum they are not affected by RF micromotion and foreign-gas collisional shifts—the two most serious and difficult to quantify frequency offsets which are present in buffer gas-cooled trapped-ion standards.

The Cs fountain scheme has been developed over recent years at the Laboratoire Primaire de Temps et Frequence, at the Observatoire de Paris into a device (OP Cs fountain, figure 35, stability performance shown in figure 19) with outstanding frequency stability and accuracy (Clairon *et al* 1995, 1996a, b, Santarelli *et al* 1995).

The effective absence of the second-order Doppler shift (table 2), due to the very low temperature of the atoms, and the low velocity with which they are launched, makes it possible to calculate very accurately the frequency offsets affecting the Cs fountain standard. The OP Cs fountain is presently reported to realize the SI second with an uncertainty not greater than ± 3 parts in 10^{15}, a level of accuracy not yet approached by any other frequency standard.

The investigation of the accuracy of the OP Cs fountain frequency standard required the study of a purely quantum mechanical effect which is unique to precision spectroscopy in ultra-cold systems (Gibble 1996, Gibble and Chu 1993, Monroe *et al* 1993, Tiesinga *et al* 1992, Verhaar *et al* 1993, Band and Julienne 1992). The extremely low temperature of the Cs atoms results in their de Broglie wavelengths being much larger than the spatial scale of their interatomic scattering potentials, which means that the cross section for collisions, and consequently the collisional frequency shift of the clock transition, is much larger than at room temperature. The cold-collisional frequency shift increases with the density of the atom cloud (figure 36), and was evaluated by extrapolating to zero atom density (Clairon *et al* 1996a, Ghezali *et al* 1996). The cold-collisional frequency shift is presently

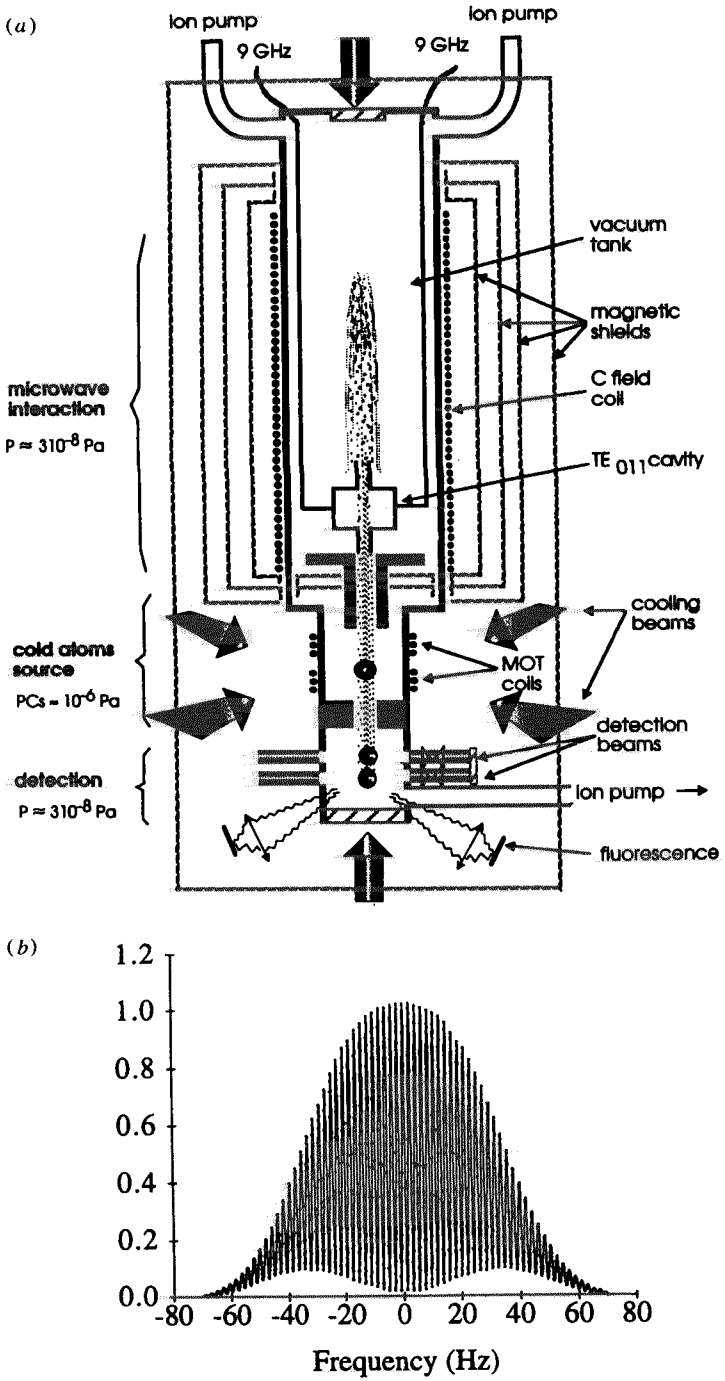

Figure 35. (*a*) Schematic of the OP ^{133}Cs fountain. The microwave cavity is located 33 cm above the cooling region (MOT/optical molasses). About 10^8 atoms are cooled to about 6 μK and launched. Due to the thermal expansion of the ion cloud, less than 10% of the atoms fall back through the microwave cavity to the detection region at the bottom of the apparatus. (*b*) Ramsey fringes separated by 1 Hz obtained by launching the atoms to a height of about 30 cm above the microwave cavity. From Clairon *et al* (1996a).

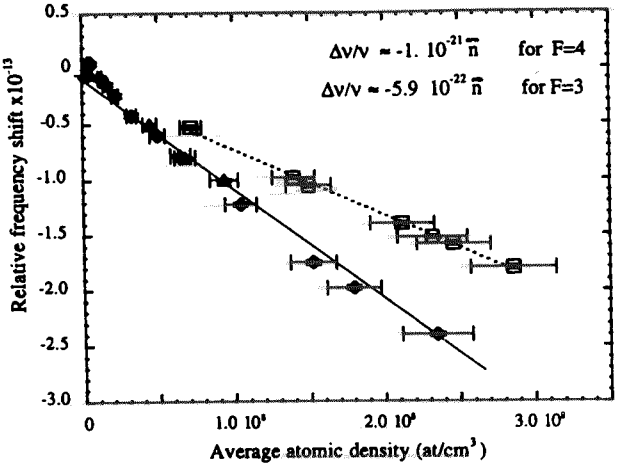

Figure 36. Fractional cold-collisional frequency shift as a function of atomic density and the state in which the atoms are prepared. From Clairon *et al* (1996a). In typical operation, the OP standard uses an average density of 5×10^5 atoms/cm^3.

a limiting factor of the SNR of the OP Cs fountain. Increasing the mean density of the clouds of atoms launched in each measurement cycle would improve the SNR, but would also introduce frequency fluctuations due to fluctuations (presently 10%) in the density of the clouds (Clairon *et al* 1996a).

Other recent developments in cold ^{133}Cs frequency standards technology include studies of schemes to minimize the collisional shift without degrading the SNR by preparing the Cs atoms in a continuous, cold, low-density atomic beam (Aucouturier *et al* 1996, Sagna *et al* 1996, Wang *et al* 1996, Yu *et al* 1991), or by timing the launching and detection of ballistic atom clouds so that several are in flight simultaneously (Ohshima *et al* 1996).

11. Limiting factors for present trapped-atom/ion standards: local oscillator requirements

The frequency stability performance, characterized by $\sigma_y(\tau)$, is limited in a number of the standards discussed above by the stability of the microwave sources (LOs) used to interrogate the atoms or ions (Clairon *et al* 1996a, b, Fisk *et al* 1996b, 1997, Rovera *et al* 1996). Over times shorter than the measurement cycle times T_c of the Cs fountain standard (about 1 s) or of the trapped-ion standards (up to 100 s or more), the inherent frequency stability of the clock transitions in the reference atoms or ions cannot be imposed on the LO. Consequently for averaging times shorter than T_c, the noise performance of the standard is, at best, that of the LO. For averaging times beyond T_c, the limitation on the frequency standard imposed by the LO depends in a rather complex way on a number of factors, including the microwave pulse sequence and LO frequency modulation scheme used to track the centre of the atomic resonance and the details of the noise properties of the LO (see, for example, Dick and Stowers 1995, Barillet *et al* 1993, 1995, Szekely *et al* 1994, Douglas and Boulanger 1992, Dick *et al* 1990, Santarelli *et al* 1996). As a simple example, the approximate limiting performance of the frequency standard (i.e. the LO–atomic reference combination), assuming an optimum pulse sequence and frequency modulation scheme, is shown graphically in figure 37.

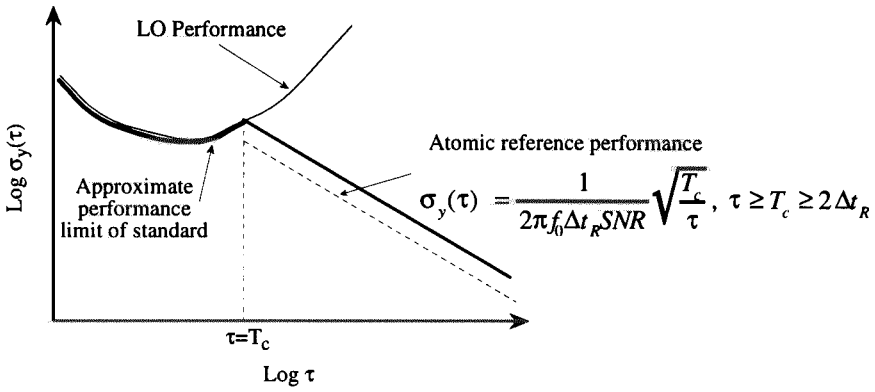

Figure 37. One way in which the performance of an atomic frequency standard is limited by the LO. Because the stability of the LO averaged over the cycle time of the standard is poorer than that of the atomic reference, the potential performance of the atomic reference is not realized.

If the microwave signal illuminates the reference atoms or ions for a time short compared with Δt_R, as in the OP Cs fountain, LO frequency fluctuations occurring over these shorter time scales can be 'down converted' in frequency and result in the degradation of the performance of the frequency standard over time scales of T_c and longer. This down conversion is known as the Dick effect (Dick *et al* 1990), and can cause degradation of the performance of the frequency standard in addition to that shown in figure 37.

Consequently, the development of a new generation of microwave oscillators with extremely good short-term stability is currently being undertaken for frequency standards and other applications by various groups (see, for example, Santiago and Dick 1993, Taber and Flory 1995, Luiten *et al* 1995a, b). These oscillators are based on resonant microwave modes of a sapphire boule cooled close to liquid nitrogen temperature (77 K) or liquid helium temperature (4.2 K), and have only recently been used as an LO for an atomic frequency standard (Prestage *et al* 1992b, Fisk *et al* 1995b).

12. Conclusion

The reader will by now have realized that trapped-atom and trapped-ion frequency standards are still at an early stage of development. There are no such standards commercially available, and only one trapped-atom frequency standard (the OP Cs fountain) has so far been demonstrated and studied in detail. Consequently these areas of research and development will continue to be interesting both from a physical and a technological point of view. For example, as the accuracy of these standards continues to improve beyond the 10^{-15} level, our understanding of the physics governing the interaction of an atom and its environment may be called into question.

An obvious question also arises. Will trapped atoms eventually be more widely used as microwave frequency standards than trapped ions, or will both technologies be used in parallel, much as the conventional caesium beam standards, hydrogen masers and rubidium standards are used today? There is no answer to this question at this time, since each technology has its advantages and disadvantages. For example, the accuracy of the Cs fountain standard presently seems unlikely to be challenged by the accuracy of buffer-gas-cooled trapped-ion standards. However, the accuracy of laser-cooled trapped-ion standards may well surpass that of the Cs fountain, but long integration times may be necessary to

realize this accuracy. To further confuse the issue, it is possible that the potential short-term stability of buffer-gas-cooled trapped-ion standards may be superior to that of Cs fountain standards.

Perhaps the most likely scenario is that several of the various trapped-atom/ion technologies will find long-term applications according to their short/long-term stability performance, their accuracy, their cost, their reliability, their size and their weight. It is also very likely that there will eventually be a move towards trapped-atom/ion optical frequency standards when a reliable and cost-effective phase-coherent link (presently under development in several laboratories) between the optical and microwave regions of the electromagnetic spectrum becomes available.

The development of the physics and engineering of the above technologies is therefore likely to continue, probably at an increasing pace driven by projected scientific and industrial requirements, for at least the next decade.

Acknowledgments

The author is grateful to Dr K G H Baldwin, Mr P E Ciddor, Dr P Hariharan, Dr Chr Tamm, Dr C J Walsh and particularly Mr M A Lawn for their constructive criticism of the manuscript as well as other assistance.

References

Allan D W 1987 *IEEE Trans. Ultrason., Ferroelectr. Freq. Contr.* **34** 647–54

Allen L and Eberly J H 1975 *Optical Resonance and Two-level Atoms* (New York: Wiley)

Aucouturier E, Dimarcq N, Petit P, Valentin C and Weyers S 1996 *Proc. 1996 European Frequency and Time Forum* (Stevenage: IEE) pp 230–3

Audoin C 1997 *Metrologia* to appear

Band Y B and Julienne P S 1992 *Phys. Rev.* A **46** 330–43

Barillet R, Giordano V, Viennet J and Audoin C 1993 *IEEE Trans. Instrum. Meas.* **42** 276–80

Barillet R, Venot D and Audoin C 1995 *Proc. 1995 IEEE Int. Frequency Control Symp.* pp 178–84

Barwood G P, Edwards C S, Gill P, Huang G, Klein H A and Rowley W R C 1995 *IEEE Trans. Instrum. Meas.* **44** 117–19

Batygin V V, Kupriyanov D V, Platonov K Y and Sokolov I M 1992 *Quantum Opt.* **4** 355–78

Bauch A, de Boer H, Fischer B, Heindorrf T and Schröder R 1988 *Proc. 42nd Annual Frequency Control Symp.* pp 490–5

Bauch A, Fischer B, Heindorrf T and Schröder R 1993a *IEEE Trans. Instrum. Meas.* **42** 444–7

Bauch A, Schnier D and Tamm Chr 1992 *J. Mod. Opt.* **39** 389–401

——1993b *Proc. 7th European Frequency and Time Forum* pp 583–8

——1996 *Proc. 5th Symp. on Frequency Standards and Metrology* (Singapore: World Scientific) pp 387–8

Bergquist J C, Itano W M, Wineland D J, Diedrich F, Elsner F and Raizen M G 1991 *Proc. 45th Annual Symp. on Frequency Control* pp 534–8

Blatt R, Casdorff V, Enders V, Neuhauser W and Toschek P E 1989 *Proc. 4th Symp. of Frequency Standards and Metrology* (Berlin: Springer) pp 306–11

Blatt R, Gill P and Thompson R C 1992 *J. Mod. Opt.* **39** 193–200

Blatt R, Schnatz H and Werth G 1982 *Phys. Rev. Lett.* **48** 1601–3

Blümel R, Kappler C, Quint W and Walther H 1989 *Phys. Rev.* A **40** 808–23

Bollinger J J, Gilbert S L, Itano W M and Wineland D J 1989 *Proc. 4th Symp. of Frequency Standards and Metrology* (Berlin: Springer) pp 319–25

Bollinger J J, Heinzen D J, Itano W M, Gilbert S L and Wineland D J 1991 *IEEE Trans. Instrum. Meas.* **40** 126–8

Bollinger J J, Itano W M and Wineland D J 1983 *Proc. 37th. Annual Frequency Control Symp.* (IEEE) pp 37–41

Bollinger J J, Prestage J D, Itano W M and Wineland D J 1985 *Phys. Rev. Lett.* **54** 1000–3

Casdorff R, Enders V, Blatt R, Neuhauser W and Toschek P E 1991 *Ann. Phys.* **7** 41–55

Clairon A, Ghezali S, Santarelli G, Laurent Ph, Lea S, Bahoura M, Simon E, Weyers S and Szymaniec K 1996a *Proc. 5th Symp. on Frequency Standards and Metrology* (Singapore: World Scientific) pp 49–59

Clairon A, Ghezali S, Santarelli G, Laurent Ph, Simon E, Lea S, Bahoura M, Weyers S and Szymaniec K 1996b *Proc. 1996 European Frequency and Time Forum* pp 218–23
Clairon A, Laurent P, Santarelli G, Ghezali S, Lea S N and Bahoura M 1995 *IEEE Trans. Instrum. Meas.* **44** 128–31
Clairon A, Salomon C, Guellati S and Phillips W D 1991 *Europhys. Lett.* **16** 165–70
Cohen-Tannoudji C, Dupont-Roc J and Grynberg G 1992 *Atom–Photon Interactions: Basic Processes and Applications* (New York: Wiley)
Corney A 1977 *Atomic and Laser Spectroscopy* (Oxford: Clarendon)
Cutler L S, Florey C A, Giffard R P and McGuire M D 1986 *Appl. Phys.* B **39** 251–9
Cutler L S, Giffard R P and McGuire M D 1981 *Proc. 13th Annual PTTI Application and Planning Meeting (NASA Conf. Publ. 2220)* pp 563–78
——1983 *Proc. 37th IEEE Frequency Control Symp.* pp 32–6
——1985 *Appl. Phys.* B **36** 137–42
Cutler L S, Giffard R P, Wheeler P J and Winkler G M R 1987 *Proc. 41st IEEE Frequency Control Symp.* pp 12–19
Dalibard J and Cohen-Tannoudji C 1989 *J. Opt. Soc. Am.* B **6** 2023–45
Dehmelt H G 1967 *Adv. At. Mol. Phys.* **3** 53–72
——1969 *Adv. At. Mol. Phys.* **5** 109–54
Desaintfuscien M, Schubert M, Siemers I and Blatt R 1992 *Appl. Phys.* B **54** 246
Dick G J, Prestage J D, Greenhall C A and Maleki L 1990 *Proc. 22nd Annual Precise Time and Time Interval (PTTI) Applications and Planning Meeting* pp 487–99
Dick G J and Stowers D A 1995 *Proc. 1995 IEEE Int. Frequency Control Symp.* pp 175–7
Dicke R H 1953 *Phys. Rev.* **89** 472–3
Dorenwendt K and Fischer B 1996 *Review of Radio Science 1993–1996* (Oxford: Oxford University Press) pp 3–9
Douglas R J and Boulanger J-S 1992 *Proc. 1992 IEEE Frequency Control Symp.* pp 6–26
Drullinger R E, Rolston S L and Itano W M 1996 *Review of Radio Science 1993–1996* (Oxford: Oxford University Press) pp 11–41
Enders V, Courteille Ph, Huesmann R, Ma L S, Neuhauser W, Blatt R and Toschek P E 1993 *Europhys. Lett.* **24** 325–31
Enders V, Courteille Ph, Neuhauser W and Blatt R 1992 *J. Mod. Opt.* **39** 325–34
Fisk P T H 1996 *Report of the 13th meeting of the Comité Consultatif pour la Définition de la Seconde (CCDS), Bureau Internationale des Poids et Mesures* ISBN 92-822-2146-6 p 56
Fisk P T H, Lawn M A and Coles C 1993a *Appl. Phys.* B **57** 287–91
——1993b *Proc. 1993 IEEE Int. Frequency Control Symp.* pp 139–43
Fisk P T H, Lawn M A, Coles C and Sellars M J 1997 *IEEE Trans. Ultrason., Ferroelectr. Freq. Control* **44** 344–54
Fisk P T H, Sellars M J, Lawn M A and Coles C 1995b *Appl. Phys.* B **60** 519–27
——1996a *Proc. 5th Symp. on Frequency Standards and Metrology* (Singapore: World Scientific) pp 27–32
——1996b *Proc. 1996 European Frequency and Time Forum* pp 212–17
Fisk P T H, Sellars M J, Lawn M A, Coles C, Mann A G and Blair D G 1994 *Proc. 1994 IEEE Int. Frequency Control Symp.* pp 731–8
——1995a *IEEE Trans. Instrum. Meas.* **44** 113–16
Foot C J 1991 *Contemp. Phys.* **32** 369–81
Fortson N 1987 *Phys. Rev. Lett.* **59** 988–90
Gaboriaud M N, Desaintfuscien M and Major F G 1981 *Int. J. Mass Spectrom. Ion Phys.* **41** 109–23
Gerz Ch, Roths J, Vedel F and Werth G 1988 *J. Phys. D: Appl. Phys.* **8** 235–7
Ghezali S, Laurent Ph, Lea S N and Clairon A 1996 *Europhys. Lett.* **36** 25–30
Ghosh P K 1995 *Ion Traps* (Oxford: Clarendon)
Gibble K E 1996 *Proc. 5th Symp. on Frequency Standards and Metrology* (Singapore: World Scientific) pp 66–73
Gibble K and Chu S 1992 *Metrologia* **29** 201–12
——1993 *Phys. Rev. Lett.* **70** 1771–4
Gibble K E, Kasapi S and Chu S 1992 *Opt. Lett.* **17** 526–8
Gill P, Klein H A, Levick A P, Roberts M, Rowley W R C and Taylor P 1995 *Phys. Rev.* A **52** R909–12
Hall J L, Zhu M and Buch P 1989 *J. Opt. Soc. Am.* B **6** 2194–205
Helmcke J 1996 *Review of Radio Science 1993–1996* (Oxford: Oxford University Press) pp 43–9
Hollberg L and Hall J L 1984 *Phys. Rev. Lett.* **53** 230–3
Imajo H, Urabe S, Hayasaka K and Watanabe M 1992 *Proc. 6th European Frequency and Time Forum* pp 319–22
Itano W M 1991 *Proc. IEEE* **79** 936–42
Itano W M, Bergquist J C, Bollinger J J, Gilligan J M, Heinzen D J, Moore F L, Raizen M G and Wineland D J

1993 *Phys. Rev.* A **47** 3554–70
Itano W M, Bergquist J C, Bollinger J J and Wineland D J 1995 *Phys. Scr.* T **59** 106–20
Itano W M, Bergquist J C and Wineland D J 1987 *Science* **237** 612–17
Itano W M, Lewis L L and Wineland D J 1982 *Phys. Rev.* A **25** 1233
Itano W M and Ramsey N F 1993 *Scientific American* **July** 46–53
Jardino M and Desaintfuscien M 1980 *IEEE Trans. Instrum. Meas.* **IM-29** 163–7
Jardino M, Desaintfuscien M, Barillet R, Viennet J, Petit P and Audoin C 1981b *Appl. Phys.* **24** 107–12
Jardino M, Desaintfuscien M and Plumelle F 1981a *J. Physique Suppl.* C **8** 327–38
Jardino M, Plumelle F, Desaintfuscien M and Duchene J L 1984 *Proc. 38th Annual IEEE Frequency Control Symp* p 431
Kasevich M A, Riis E and Chu S 1989 *Phys. Rev. Lett.* **63** 612–15
Klein H A, Bell A S, Barwood G P, Gill P and Rowley W R C 1991 *IEEE Trans. Instrum. Meas.* **40** 129–31
Knab H, Niebling K-D and Werth G 1985 *IEEE Trans. Instrum. Meas.* **34** 242–5
Lee W D, Shirley J H, Lowe J P and Drullinger R E 1995 *IEEE Trans. Instrum. Meas.* **44** 120–3
Lehmitz H, Hattendorf-Ledwoch J, Blatt R and Harde H 1989 *Phys. Rev. Lett.* **62** 2108–11
Lewis L L 1991 *Proc. IEEE* **79** 927–35
Luiten A N, Mann A G, Costa M E and Blair D G 1995a *IEEE Trans. Instrum. Meas.* **44** 132–5
Luiten A N, Mann A G, McDonald N J and Blair D G 1995b *Proc. 1995 IEEE Int. Frequency Control Symp.* pp 433–7
Lunney M D N, Buchinger F and Moore R B 1992 *J. Mod. Opt.* **39** 349–60
Maleki L 1981 *Proc. 13th Annual Precise Time and Time Interval (PTTI) Applications and Planning Meeting* pp 593–603
Matsakis D N, Kubik A J, DeYoung J A, Giffard R P and Cutler L S 1995 *Proc. 1995 IEEE Frequency Control Symp.* pp 86–109
Meis C, Desaintfuscien M and Jardino M 1988 *Appl. Phys.* B **45** 59–64
Meis C, Jardino M, Gely B and Desaintfuscien M 1989 *Appl. Phys.* B **48** 67–72
Metcalf M and van der Straten P 1994 *Phys. Rep.* **244** 203–86
Miller J D, Berkeland D J, Cruz F C, Bergquist J C, Itano W M and Wineland D J 1996 *Proc. 1996 Int. IEEE Frequency Control Symp.* pp 1086–8
Miller J D, Poitzsch M E, Cruz F C, Berkeland D J, Bergquist J C, Itano W M and Wineland D J 1995 *Proc. 1995 IEEE Int. Frequency Control Symp.* pp 110–12
Monroe C, Cornell E A, Sackett C A, Myatt C J and Wiemann C E 1993 *Phys. Rev. Lett.* **70** 414–17
Monroe C, Robinson H and Wieman C 1991 *Opt. Lett.* **16** 50–2
Monroe C, Swann W, Robinson H and Wieman C 1990 *Phys. Rev. Lett.* **65** 1571–4
Ohshima S, Kurosu T, Ikegami T and Nakadan Y 1995 *Japan. J. Appl. Phys.* **34** L1170–3
——1996 *Proc. 5th Symp. on Frequency Standards and Metrology* (Singapore: World Scientific) pp 60–5
Paul W 1990 *Rev. Mod. Phys.* **62** 531–40
Peik E, Hollemann G and Walther H 1995 *Phys. Scr.* T **59** 403–5
Phillips W D, Lett P D, Rolston S L, Tanner C E, Watts R N, Westbrook C I, Salomon C, Dalibard J, Clairon A and Guellati S 1991 *IEEE Trans. Instrum. Meas.* **40** 78–80
Poitzsch M E, Bergquist J C, Itano W M and Wineland D J 1994 *Proc. 1994 Int. IEEE Frequency Control Symp.* pp 744–6
——1996 *Rev. Sci. Instrum.* **67** 129–34
Prestage J D, Dick G J and Maleki L 1987a *Proc. 41st Annual Frequency Control Symp.* pp 20–4
——1987b *Proc. 19th Annual Precise Time and Time Interval (PTTI) Applications and Planning Meeting* pp 285–96
——1988 *Proc. 20th Annual Precise Time and Time Interval (PTTI) Applications and Planning Meeting* pp 305–10
——1989 *J. Appl. Phys.* **66** 1013–17
——1990a *Proc. 22nd Annual Precise Time and Time Interval (PTTI) Applications and Planning Meeting* pp 171–84
——1990b *Proc. 44th Annual Symp. on Frequency Control* pp 82–8
——1991 *IEEE Trans. Instrum. Meas.* **40** 132–6
Prestage J D, Janik G R, Dick G J and Maleki L 1990c *IEEE Trans. Ultrason., Ferroelectr. Freq. Control* **37** 535–42
Prestage J D and Maleki L 1994 *Proc. 1994 IEEE Int. Frequency Control Symp.* pp 747–54
Prestage J D, Tjoelker R L, Dick G J and Maleki L 1992a *J. Mod. Opt.* **39** 221–32
——1993a *Proc. 1993 IEEE Int. Frequency Control Symp.* pp 148–54
——1993b *Proc. 1993 IEEE Int. Frequency Control Symp.* pp 144–7
——1994 *Proc. 1994 IEEE Int. Frequency Control Symp.* pp 755–60
——1995 *Proc. 1995 IEEE Int. Frequency Control Symp.* pp 82–5

Prestage J D, Tjoelker R L, Wang R T, Dick G J and Maleki L 1992b *Proc. 1992 IEEE Int. Frequency Control Symp.* pp 58–63
Quinn T J 1991 *Proc. IEEE* **79** 894–905
Raab E L, Prentiss M, Cable A, Chu S and Pritchard D E 1987 *Phys. Rev. Lett.* **59** 2631–4
Raizen M G, Gilligan J M, Bergquist J C, Itano W M and Wineland D J 1992 *J. Mod. Opt.* **39** 233–42
Ramsey N F 1983 *J. Res. NBS* **88** 301–20
——1991 *Proc. IEEE* **79** 921–6
Rolston S L and Phillips W D 1991 *Proc. IEEE* **79** 943–51
Rovera G D, Santarelli G and Clairon A 1996 *IEEE Trans. Ultrason., Ferroelectr. Freq. Control* **43** 354–8
Rutman J and Walls F L 1991 *Proc. IEEE* **79** 952–60
Sagna N, Dudle G, Berthoud P and Thomann P 1996 *Proc. 1996 European Frequency and Time Forum* pp 224–9
Santarelli G, Ghezali S, Laurent Ph, Lea S N, Bahoura M, Szymaniec K, Simon E and Clairon A 1995 *Proc. 1995 IEEE Int. Frequency Control Symp.* pp 60–5
Santarelli G, Laurent Ph, Clairon A, Dick G J, Greenhall C A and Audoin C 1996 *Proc. 10th European Frequency and Time Forum* pp 66–71
Santiago D G and Dick G J 1993 *Proc. 1993 IEEE Int. Frequency Control Symp.* pp 774–8
Schnier D 1992 *PhD Dissertation* Physikalisch-Technische Bundesanstalt PTB-Bericht-Opt-37
Schnier D, Bauch A, Schröder R and Tamm Chr 1992 *Proc. 6th European Frequency and Time Forum* pp 415–20
Schubert M, Siemers I and Blatt R 1990 *Appl. Phys.* B **51** 414–17
Seidel D J and Maleki L 1994 *Proc. 1994 IEEE Int. Frequency Control Symp.* pp 761–8
——1995a *Proc.1995 IEEE Int. Frequency Control Symp.* pp 74–8
——1995b *Phys. Rev.* A **51** R2699
Seidel D J, Williams A, Berends R W and Maleki L 1992 *Proc. 1992 IEEE Frequency Control Symp.* pp 70–5
Sellars M J, Fisk P T H, Lawn M A and Coles C 1995 *Proc. 1995 IEEE Frequency Control Symp.* pp 66–73
Sesko D W and Wieman C E 1989 *Opt. Lett.* **14** 269–71
Shen Y R 1984 *The Principles of Nonlinear Optics* (New York: Wiley)
Sugiyama K and Yoda J 1992 *Hyperfine Interact.* **74** 251–8
——1993 *IEEE Trans. Instrum. Meas.* **42** 467–73
——1995 *Japan. J. Appl. Phys.* **34** L584–6
——1997 *Phys. Rev.* A **55** R10–13
Sullivan D B and Levine J 1991 *Proc. IEEE* **79** 906–14
Szekely C, Walls F L, Lowe J P, Drullinger R E and Novick A 1994 *IEEE Trans. Ultrason., Ferroelectr. Freq. Control* **41** 518–21
Taber R C and Flory C A 1995 *IEEE Trans. Ultrason., Ferroelectr. Freq. Control* **42** 111–19
Tamm Chr 1993 *Appl. Phys.* B **56** 295–300
Tamm Chr and Schnier D 1992 *Opt. Commun.* **87** 240–4
Tamm Chr, Schnier D and Bauch A 1995 *Appl. Phys.* B **60** 19–29
Tan J N, Bollinger J J and Wineland D J 1995 *IEEE Trans. Instrum. Meas.* **44** 144–7
Tanaka U, Imajo H, Hayasaka K, Ohmukai R, Watanabe M and Urabe S 1996 *Phys. Rev.* A **53** 3982–5
Tiesinga E, Verhaar B J, Stoof H T C and van Bragt D 1992 *Phys. Rev.* A **45** R2671–3
Tjoelker R L *et al* 1996b *Proc. 1996 IEEE Int. Frequency Control Symp.* pp 1073–81
Tjoelker R L, Prestage J D, Dick G J and Maleki L 1993 *Proc. 1993 IEEE Int. Frequency Control Symp.* pp 132–8
——1994 *Proc. 1994 IEEE Int. Frequency Control Symp.* pp 739–43
Tjoelker R L, Prestage J D and Maleki L 1995 *Proc. 1995 IEEE Int. Frequency Control Symp.* pp 79–81
——1996a *Proc. 5th Symp. on Frequency Standards and Metrology* (Singapore: World Scientific) pp 33–8
Vanier J and Audoin C 1989 *The Quantum Physics of Atomic Frequency Standards* (Bristol: Hilger)
Verhaar B, Gibble K and Chu S 1993 *Phys. Rev.* A **48** R3429–32
Wang Y, Li Y, Gan J, Chen X and Yang D 1996 *Proc. 5th Symp. on Frequency Standards and Metrology* (Singapore: World Scientific) pp 74–80
Werth G 1985 *IEEE Trans. Instrum. Meas.* **34** 238–45
——1987 *Hyperfine Interact.* **38** 699–709
Wineland D J *et al* 1996 *Proc. 5th Symp. on Frequency Standards and Metrology* (Singapore: World Scientific) pp 11–19
Wineland D J 1981 *Proc. 13th Annual PTTI Application and Planning Meeting (NASA Conf. Publ. 2220)* pp 579–91
——1984 *Science* **226** 395–400
Wineland D J, Bergquist J C, Bollinger J J, Itano W M, Heinzen D J, Gilbert S L, Manney C H and Raizen M G 1990b *IEEE Trans. Ultrason., Ferroelectr. Freq. Control* **37** 515–23
Wineland D J, Bollinger J J, Itano W M and Heinzen D J 1994 *Phys. Rev.* A **50** 67–88

Wineland D J, Bollinger J J, Itano W M and Moore F L 1992 *Phys. Rev.* A **46** R6797–800
Wineland D J and Itano W M 1983 *Adv. At. Mol. Phys.* **19** 135–86
——1987 *Phys. Today* **June** 34–40
Wineland D J, Itano W M, Bergquist J C, Bollinger J J, Diedrich F and Gilbert S L 1989 *Proc. 4th Symp. of Frequency Standards and Metrology* (Berlin: Springer) pp 71–7
Wineland D J, Itano W M, Bergquist J C, Bollinger J J, Heinzen D J, Manney C H, Moore F L, Raizen M G and Weimer C S 1990a *Proc. 22nd Annual PTTI Application and Planning Meeting (NASA Conf. Publ. 3116)* p 53
Wineland D J, Itano W M, Bergquist J C and Hulet R G 1987 *Phys. Rev.* A **36** 2220–32
Wineland D J, Itano W M, Bergquist J C and Walls F L 1981 *Proc. 35th Annual Frequency Control Symp.* pp 602–11
Yoda J and Sugiyama K 1992a *Japan. J. Appl. Phys.* **31** 3750–3
——1992b *J. Mod. Opt.* **39** 403–9
Yu J, Guellati S, Gagné M-C, Clairon A and Picqué J-L 1991 *Opt. Commun.* **82** 27–33